ABSTRACT

MARTIN, TIMOTHY NEIL. Nanoporous and Thin Film Gold and Silver Metal Alloys and Their Medical Applications in Drug Delivery and Antimicrobial Properties. (Under the direction of Dr. Roger J. Narayan).

Gold and silver alloys have become popular biomaterials because they offer good electrochemical properties, antimicrobial properties, and biocompatibility. In this study, electrochemically etched wires as well as alloy thin films were prepared. Gold nanoporous materials have been shown to exhibit supercapacitive behavior when placed in contact with charged particles in solution. The medical applications of nanoporous gold have ranged from pharmaceutical-controlled release to gene delivery. A method for making gold nanoporous material has been demonstrated that involves galvanically etching gold and silver alloys in order to selectively remove silver from the alloy, which results in a porous material.

It was hypothesized that by leaving specific amounts of silver in the alloy material, the nanoporous material could provide the benefits of a supercapacitive material as well as the benefits of a silver-rich material that would act as an antimicrobial agent. In order to analyze the alloy metals in the range of antimicrobial testing, thin film samples were deposited using pulsed laser deposition of alloys onto silicon wafer substrates. The nanoporous wires and thin film alloys were tested using energy dispersive X-ray spectroscopy, X-ray diffraction, scanning electron microscopy, Kirby-Bauer disk diffusion susceptibility testing, and potentiostat controlled cyclic voltammogram. The results showed that supercapacitive wires that exhibited impressive antimicrobial activity. Several wires were created in which the percentage of silver remaining in the samples was varied. The wires were shown to exhibit porous structures and regions that would be classified as nanoporous. The results suggest that nanoporous gold materials can be produced that retain

silver and exhibit antimicrobial properties; these materials have potential use in a wide range of biomedical applications.

Nanoporous and Thin Film Gold and Silver Metal Alloys and Their Medical Applications in Drug Delivery and Antimicrobial Activity

by
Timothy Neil Martin

A thesis submitted to the Graduate Faculty of
North Carolina State University
in partial fulfillment of the
requirements for the Degree of
Master of Science

Biomedical Engineering

Raleigh, North Carolina

2012

APPROVED BY:

_____	_____
Dr. A. Banes	Dr. N. Monteiro-Riviere
_____	_____
Dr. R. Narayan Chair of Advisory Committee	Dr. Y. Lee

DEDICATION

To Emily.

BIOGRAPHY

Timothy Martin attended North Carolina State University as an undergraduate and received a Bachelor of Science in Biomedical Engineering in 2010.

ACKNOWLEDGEMENTS

Thank you to Dr. Roger Narayan for being my advisor, mentor and lab leader. I would not be in graduate school if not for Dr. Narayan. Thank you Dr. David Robinson who trained me at Sandia National Laboratory in Livermore, California for all the electrochemical processes. Thank you Dr. Reza Bayati for helping me with the PLD process and being patient enough for me to finish. Thank you to everyone at the AIF at NCSU: Chuck Mooney, Dale Bachelor, Jonathan Pierce, and Roberto Garcia. Without their help none of my results would have been possible.

TABLE OF CONTENTS

LIST OF FIGURES

LIST OF TABLES

I. INTRODUCTION

Nanoporous gold has unique medical properties, which enable it to store and release drugs under electronic control; pre-concentrate analytes; bind cells; as well as pass nutrients and signals to cells. A recent report has stated that the market potential for nanomaterials in biotechnology and medicine in 2015 is estimated to be around 6.2 billion US dollars (Global Industry Analysts 2010). Nanoporous materials are an intriguing subject area because of their wide ranging applications. Research has been focused on medical areas (e.g., drug delivery and biosensors) as well as on energy storage and other alternative energy technologies. This thesis will highlight current information regarding medical applications of nanoporous gold as well as the impact of residual silver in the alloy. The main focus of this introduction and background is to present the latest medical applications of nanoporous gold and silver, methods for processing the material, and characterization of the material.

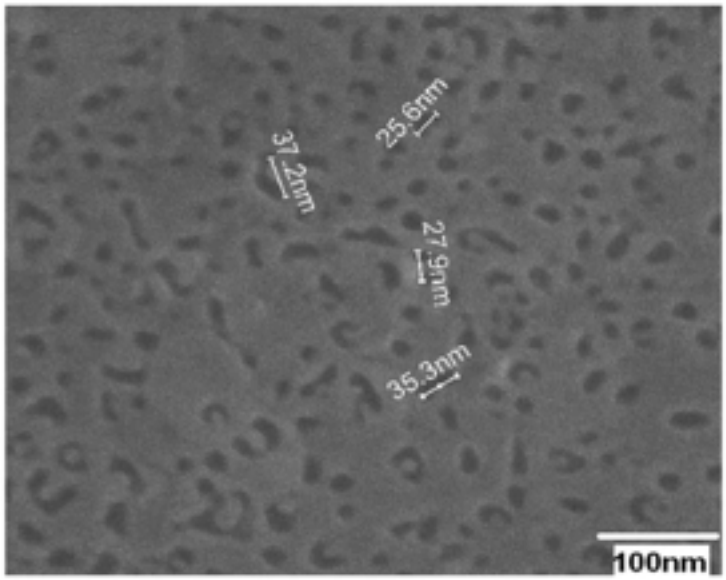

Figure 1. SEM image of typical nanoporous gold ($Ag_{58}Au_{42}$) with average pore size of 34 nm. Reprinted from Microelectronic Engineering, 88, Quan X, Fischer L, Boisen A, Tenje M, Development of nanoporous gold electrodes for electrochemical applications, 2379-2382, Copyright (2011), with permission from Elsevier.

In order to properly understand the advantages of nanoporous gold in medical applications, it is necessary to understand the limitations of other materials that are currently being used. Polymers with various structures have been used for many years in pharmaceutical delivery and other biological applications. Polymers exhibit many appropriate characteristics for designing novel sensors or delivery vehicles because of their adaptable designs. One approach to make a porous polymer with precisely sized pores is to construct a composite material and remove the polymeric material that is not desired.

Another approach to removing polymeric material involves sending high-energy ions through a polymer membrane and then dissolving the degraded polymeric material; this approach is used to create ion track etched polymer membranes.

Nanofiber and nanotube polymers can be used in drug delivery and biosensing. The most common method for making both porous and hollow polymer nanofibers is through electrospinning. The process of electrospinning deals with applying a strong electric field to a stream of polymeric material (Dersch 2005). Typically, the tip of the die acts as one electrode and the counter electrode is located approximately 10 centimeters away (Dersch 2005). The electrical field between the two electrodes causes the stream of polymer to thin as it approaches the counter electrode (Dersch 2005). The solvent evaporates during this portion of the process, resulting in solid polymer deposition on the counter electrode and a random orientation of fibers (Dersch 2005). In order to make a porous fiber mesh, the electrospinning process involves two different polymer types. Once deposited, one of the polymers is selectively removed in a solvent bath, resulting in a porous structure that is similar the structure shown in Figure 2 (Dersch 2005).

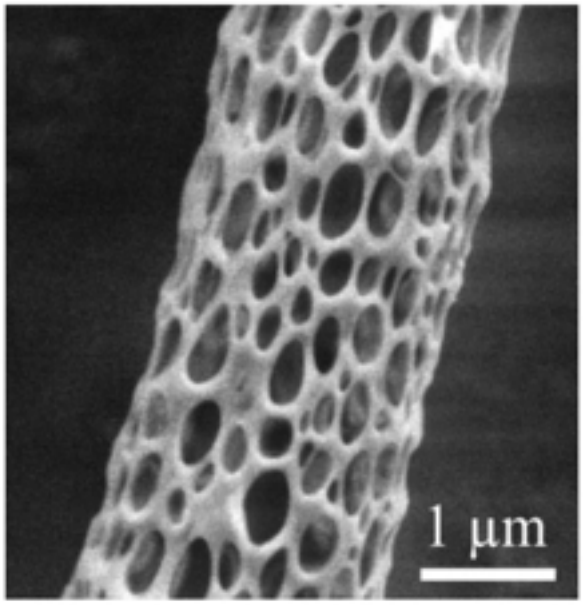

Figure 2. Poly lactic acid fiber with porous surface spun from dicholoromethane. Reprinted from Dersch R, Steinhart M, Boudriot U, Greiner A and Wendorff J (2005), 'Nanoprocessing of polymers: applications in medicine, sensors, catalysis, photonics', *Polymers for Advanced Technologies*, 16, 276-282. Copyright © 2005 John Wiley & Sons, Ltd.

In addition to polymer removal, co-electrospinning has been developed to create a core-shell polymer fiber. The process of electrospinning is modified to have a core nozzle that is surrounded concentrically by an array of outer shell nozzles (Dersch 2005.) The resulting fibers consist of two separate polymer types, which are located on the interior and exterior of the fiber. Uses for this type of polymer primarily involve drug delivery. The core polymer can be impregnated with a time-release pharmaceutical; the shell polymer provides structural support. The advantages of electrospun polymers are relative control over the final polymer constituents and uniform fiber dimensions. The disadvantages to electrospun polymers are that they require the use of a very high electrical potential, the fiber mesh is

randomly deposited, and the mechanical properties widely vary depending on the polymer that is used.

Ion track etched polymers are another type of material with similar characteristics and applications to nanoporous gold. Ion track etched materials can be used in various medical applications, including biosensor applications. Because ion track etched polymers exhibit pores with uniform diameters as well as a uniform pore layout, these materials are commonly utilized in biosensor applications (Alfonta 2009). Biosensors require pores that are similar in size and shape in order to detect analytes in blood in a reproducible manner. Ion track etching is a widely used technique that is commercially utilized to create products such as filters, printed circuit boards, and heat exchangers (Spohr 2005).

To exploit the benefits of the ion track etched material, the majority of research has focused on developing techniques that precisely count analytes that pass through the pores of a membrane. There are several different ways to count particles passing through a pore; one of these techniques uses the Coulter principle. Deblois and Bean successfully transferred this approach from glass capillaries to ion etched pores in 1970 (Spohr 2005). Some other novel uses of ion track technology include gating pores and integrating tracks into microfluidic devices (Spohr 2005). Gating pores involves having electronic control of a physical gate that can open or close depending on the potential that is applied. The advantage to gating pores is that a researcher can precisely control what particles are allowed in and out of a specific pore on the membrane. Also, the researcher can set up single molecule-sized passageways with ion track etched methods for microfluidic devices.

Glucose detection is by far the most popular use of biosensors; however, track etched membrane technology can be applied for monitoring of various analytes in the body. Alfonta documented the current status of ion track etched biosensors, tabulated the process for creating these biosensors, as well as discussed reusable and non-reusable designs. Track etched biosensors mainly include nanoporous biofunctionalized membranes made of polyimide, nanoporous biofunctionalized membranes made of polyethylene terephthalate, nanoporous biofunctionalized membranes made of polycarbonate, and nanoporous semiconductor-insulator bilayer materials.

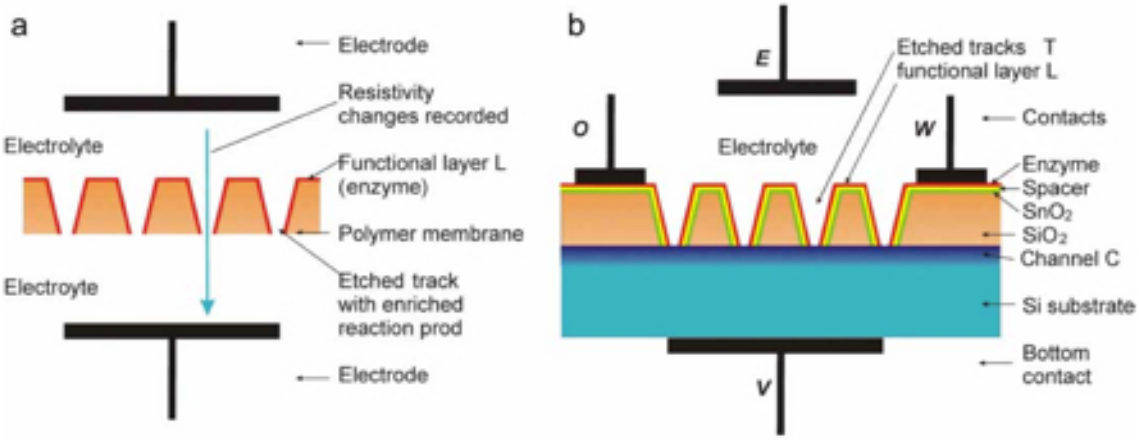

Figure 3. Biosensors created with ion track etched materials (a. nanoporous biofunctionalized membrane b. membrane-semiconductor bilayer structures with biofunctionalized layer deposited on ion track walls). Reprinted from Alfonta L, Bukelman O, Chandra A, Fahrner W, Fink D, Fuks D, Golovanov V, Hnatowicz V, Hoppe K, Kiv A, Klinkovich I, Landau M, Morante J, Tkachenko N, Vacik J, Valden M (2009), 'Strategies toward advanced ion track-based biosensors', *Radiation Effects & Defects in Solids*, 164, 431-437 with permission from Taylor & Francis Ltd. (http://www.informaworld.com).

The initial design of a track etched biosensor is noted in Figure 3a and consists of a conical track etched polymer membrane with a gold nanotube inserted within it (Alfonta 2009). Bioactive substances such as enzymes or other molecules that interact with biomolecules are placed inside the gold nanotubes. During detection, proteins or other biomolecules of note are captured in the nanotube, where they alter the resistance of the nanotube. The resistance change is related to biomolecule characteristics, enabling the specific molecule to be precisely determined. The major disadvantage is that the nanotube can only detect one biomolecule and it cannot be reused. Because of its limited functionality, this design was not favored; it has been replaced by the membrane-semiconductor bilayer structure shown in Figure 3b.

The bilayer structure is regarded as a tunable electronic material in which pores are located in an oxide on a semiconductor (TEMPOS) (Alfonta 2009). The basic structure consists of a polymer foil that has undergone ion track etching; a coating of semiconductor is located on the functional surface. Enzymes or other bioactive substances are applied to the walls of the pore (Alfonta 2009). The principal mechanism of action is similar to that of the nanotube –modified single track etched polymer. The main advantage compared to the previously described design is that it can be reused as long as the enzyme is retained on the pore walls. Also, measurements are much easier to obtain because current ranges are much higher than in the single use design (Alfonta 2009). The disadvantage is that the TEMPOS design is not as sensitive as the nanotube –modified single track etched polymer design (Alfonta 2009).

Nanoporous gold and silver alloys will be used in many of the same ways that the polymers have been described. The important area of interest for this thesis is to investigate the ability to produce the nanoporous material with both gold and silver present and to characterize the ability to have antimicrobial activity as well as electrical properties inherent to nanoporous metals. It will also be investigated if the ability to create thin films with varying quantities of gold and silver will produce similar antimicrobial results.

Hypothesis:

Nanoporous gold and silver alloys in both thin films and electrochemically produced wires exhibit electrical properties for drug delivery as well as antimicrobial activity that would prove beneficial for use in medical applications.

Objectives:

- Electrochemically produce nanoporous metal alloys with gold and residual silver content
- Electrochemically characterize the nanoporous alloys for drug delivery applications as well as show antimicrobial action greater than non-porous materials
- Produce thin films of gold and silver alloys with a range of silver content in a reliable and reproducible method
- Measure antimicrobial activity, purity, and surface characterization of the thin film alloys

II. BACKGROUND

1. NANOPOROUS METALS

Nanoporous gold is a versatile material that can be used in many areas. This section will focus on how nanoporous gold can be used for medical applications. Because of its inherent biocompatibility and inert nature, gold can be used in almost any region of the human body. Gittard (2010) proposed using nanoporous gold in a supercapacitive array inside of hollow microneedles for both drug delivery and biological monitoring. Sperling (2008) wrote an extensive review on biological applications of gold nanoparticles, in which many of the advantages and properties of nanoporous gold are discussed. Nanoporous gold has very unique chemical and biological properties that enable its use in many different areas of medicine.

Gittard (2010) described a process for incorporating nanoporous gold wires within microneedles for drug delivery. The main idea that Gittard was investigating was the ability to leverage the high surface area of nanoporous gold by adsorbing a pharmaceutical onto it and then precisely delivering it to the patient from a microneedle. The study focused on exploiting the supercapacitive characteristics of nanoporous gold and involved creating nanoporous wires, loading the wires with the desired drug, rinsing in water, and then discharging in a competitive environment. Cyclic voltammetry (CV) is a method of electrochemical detection that involves ramping the voltage applied to the cell up and then down in order to understand the behavior of the current flowing through the cell. Figure 4 depicts CV data from nanoporous gold material that has been exposed to a potential ramp

from 0 mV to +200 mV to -200 mV and back to 0 mV (Gittard 2010). The analyte used for this test was sodium trifluoroacetate (TFA) because of the relatively equal charge mobility of sodium and TFA molecule. The CV data shows that the gold material has capacitive characteristics because of the large area between the voltage sweep up and then down; in addition, relatively constant current during each sweep was noted. Overall, Gittard was able to show high capacitance and the ability to repeatedly charge and discharge the target drug. The next steps for this approach would be to look into clinical applications involving microneedles and to provide larger volumes of pharmaceutical to the microneedles by means of a microfluidic array.

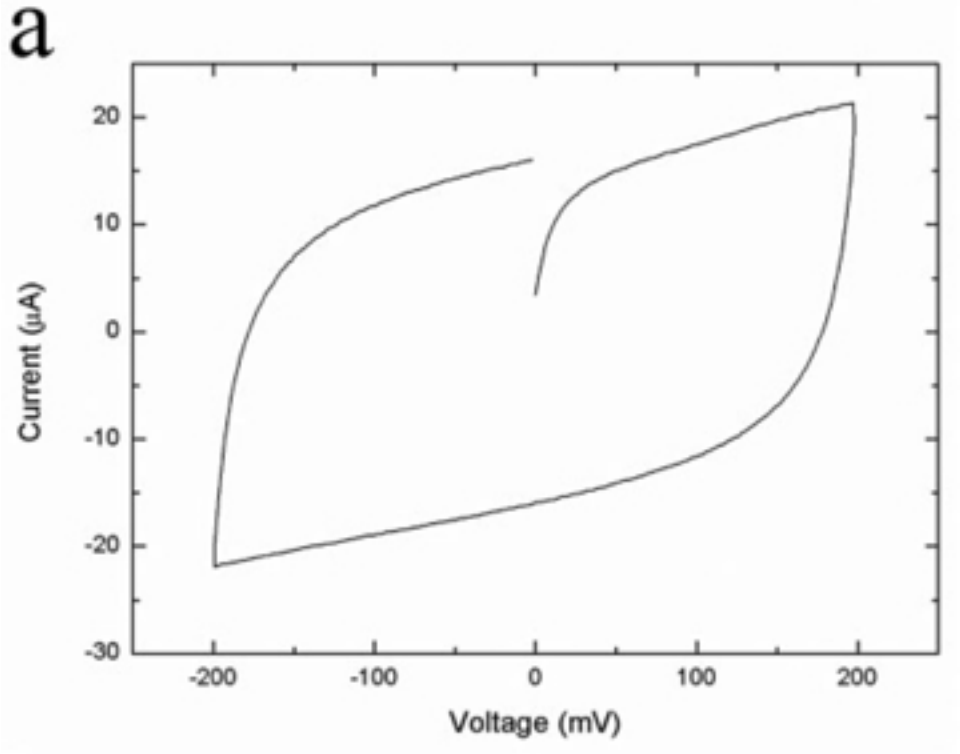

Figure 4. Cyclic Voltammogram of sodium trifluoroacetate solution with the nanoporous gold material. Reprinted from Gittard S, Pierson B, Ha C, Wu C, Narayan R and Robinson D (2010), 'Supercapacitive transport of pharmacologic agents using nanoporous gold electrodes', *Biotechnology Journal*, 5, 192-200. Copyright © 2010 Wiley-VCH Verlag GmbH & Co. KGaA, Weinheim.

An important characteristic of gold in nanoporous and nanoparticle form is that it is considered to be biocompatible. Several investigations have taken place to analyze the effect of nanoscale gold on the human body. Pedersen (2009) investigated the effect of gold on inflammation and healing, which involved inducing traumatic brain injury through application of dry ice to an exposed extracranial section of the skull for 30 seconds. After the

injury was completed, a solution of sodium hyaluronate and gold particles was injected into the wound site (Pedersen 2009). Autometallography was used to evaluate gold nanoparticles migration over two weeks (Pedersen 2009). Pedersen was able to show that gold increased proliferation of cells in brain tissue, specifically in the contralateral subventricular region and in the ipsilateral region of the murine model. In addition, the histological and cell signaling data from the study suggest that inflammation was reduced (Pedersen 2009). Overall, the gold nanoparticle was beneficial in all portions of healing with a traumatic brain injury. The treatments decreased inflammation, increased expression of important regenerative growth factors, and stimulated migration of neural stem cells for growth of new brain tissue.

Sperling (2008) described the use of gold nanoparticles for labeling and visualizing various biological functions. The inherent properties of gold as a good conductor of electricity and as an easily resolved material in a variety of techniques such as transmission electron microscopy and optical microscopy are the main reasons why gold is a useful tracking material. Immunostaining is one use of gold nanoparticles; this process involves conjugating gold with antibodies that will react with biomolecules of interest (Sperling 2008). Single particle tracking is also possible by utilizing only a small number of gold nanoparticles containing a specific marker (Sperling 2008). The gold nanoparticles will then track the target biomolecule and allow for facile detection. Gold nanoparticles can also be used to deliver various biologically-relevant molecules. Gene guns are one example of this approach; DNA molecules are attached to the surface of the gold nanoparticles and are fired into the desired region of the body using gas pressure and electronic discharge (Sperling

2008). Another important use of this delivery mechanism involves uptake of gold nanoparticles into the targeted cell and then release of the attached molecules within the cell. Gold is also unique in that it benefits from facile modification; a wide range of potential attachment molecules can be incorporated due to thiol-gold bonding (Sperling 2008). Some care is needed when selecting the appropriate nanoparticle attachment in order to correctly direct the cell to accept the particle and to correctly unpackage the attached molecule within the correct organelle. Gold nanoparticles are not necessarily nanoporous but have been considered for use in a variety of medical applications over the years.

Several important medical applications of nanoporous gold involve the field of biosensing. Biosensing involves using one or more assays (e.g., electrochemistry and optical assays) to detect biological molecules, markers, or identifiable processes. Many biosensors that incorporate nanoporous gold involve enzyme-based monitoring of glucose oxidase for detection of glucose. Also, nanoporous gold can be grown onto another biocompatible metal, titanium; hydrogen peroxide activity can be monitored through affixing hemoglobin to the nanoporous surface. Nanowires, which have some characteristics similar to those of nanoporous gold, can also be used for biosensing. In addition, use of a nanoporous gold film for glucose monitoring will be explained.

Horseradish peroxidase is the enzyme that is most frequently used for glucose detection because of its ability to amplify weak biological signals (e.g., the amount of hydrogen peroxide in blood). Researchers have investigated the ability of hemoglobin in place of horseradish peroxidase for monitoring the concentration of hydrogen peroxide.

There is a need to find a suitable replacement for horseradish peroxidase because of its high cost and instability. The amount of hydrogen peroxide in a sample directly correlates with the amount of glucose in the sample. Kafi (2010) successfully used hemoglobin for monitoring hydrogen peroxide levels. A linear range of 5.0×10^{-8} M - 2.0×10^{-4} M was obtained for hemoglobin; in comparison, horseradish peroxidase with carbon nanotubes provided a range of 4.0×10^{-6} M - 2.0×10^{-3} M. The stability was also impressive, matching horseradish peroxidase/Au/ TiO_2 nanotubes with 95% stability after 45 days.

Due to the difficulty in controlling the parameters that enable a consistent and accurate reading to be obtained from an enzymatic electrode, there is an advantage in using a non-enzymatic electrode for glucose monitoring. Temperature, pH, and humidity can cause an enzyme-based system to provide incorrect glucose concentration measurements (Xia 2011). Nanoporous gold was shown to be better than smooth gold for quantifying the glucose concentration. Instead of detecting the activity of glucose oxidase with horseradish peroxidase, Xia (2011) described creating an AuOH intermediate on the surface of the film. Another advantage associated with using an enzyme-free approach was the reduction in interference by ascorbic acid or uric acid (Xia 2011). The approach described by Xia showed competitive sensitivity and a wide linear range for detecting glucose in the tested samples.

The most commonly evaluated approach for measuring glucose involves applying glucose oxidase to the surface of an electrode. Qiu (2009) used glucose oxidase for glucose detection and alcohol dehydrogenase for ethanol detection with nanoporous gold electrodes. Cyclic voltammagrams showed the increased capacitance and overall increase in

performance with glucose oxidase -modified nanoporous gold. An advantage to using nanoporous gold electrodes is that this material can be used over many cycles without a loss in performance. Unlike gold nanoparticles in solution, nanoporous gold electrodes do not have to be recovered from solution.

This section will describe use of dealloying to create nanoporous gold. In order to create a porous material, silver, zinc and/or other metal components of a gold alloy are removed in varying amounts. To form a gold alloy, the components can be melted together to form an ingot, electronically sputtered into a surface coating, ion sputtered, electroplated, or chemically reduced. The preferred percentage of gold in gold alloys used for dealloying is usually 20-40 % atomic weight because this composition is associated with optimal dealloying characteristics (Kertis 2010). A furnace can be used to melt the two metals into a homogeneous solid under an argon gas environment, which serves to limit oxidation (Kertis 2010). Arc melting can also be used to form an alloy from the component metals; temperatures up to 1223 K and processing times of over 70 hours may be used (Jin 2009). Quan (2011) described using sputtering in order to form gold-silver alloys. Gold and silver were sputtered onto a silicon wafer in various combinations; alloys with a gold concentration of 34-45% and a silver concentration of 55-64% were obtained using this approach (Quan 2011). Dong (2008) showed that alloys containing gold and zinc can be created by plating Zn/Au onto a sputtered gold surface. Kafi (2010) also used sputtering to grow a nanoporous gold film on a titanium plate. Seker (2007) electroplated various metals onto a silicon wafer; dealloying was performed to create nanoporous gold beams that were used for mechanical

testing. One interesting method to create gold alloy was described by Liu (2006), which involved preparing a template, electrodepositing the alloy into the template, and then chemically removing the template to reveal alloy nanowires. This precise template provides significant control over nanowire geometry and enables formation of innovative nanowire designs. Efforts are also underway to toughen and strengthen gold alloys. For example, Senior (2006) demonstrated annealing of alloy sheets at 975º C for one hour under hydrogen gas.

Dealloying of the gold and silver alloy is usually accomplished in one of two ways: acid etching or electrochemical etching. Acid corrosion is a chemically straightforward process that is used for selective removal of silver. The most common method for dealloying with acid alone involves immersing the sample in concentrated nitric acid (69% HNO_3) for a specified period of time. Effective etching of the alloy can be performed in a short amount of time, usually between two and ten minutes (Quan 2011). Work by Biener has shown advantages to keeping the alloy in solution for two to five days (Biener 2006). After being removed from the acid, the sample is extensively washed with deionized water to remove the remaining acid and reaction byproducts. Nitric acid is commonly used for dealloying because silver is easily oxidized to a nitrate salt whereas gold is not. The result of free corrosion is a porous material with a pore size in the 10-15 nm range (Kertis 2010). One way to modify nitric acid-based dealloying is to increase the temperature. Seker (2007) showed that samples annealed at higher temperatures possessed higher relative density measurements, higher residual stress values, and higher elastic modulus values. Another

popular type of free corrosion was discussed by Cattarin (2007), which involved using 1 M perchloric acid ($HClO_4$) to remove the silver from the alloy over a period of approximately three hours. One advantage of the free corrosion process is its simplicity. The disadvantage to this method is the lack of precise control over the pore size and inability to control the porosity beyond the surface of the material. There are two additional variables that can provide control over the dealloying process for acid corrosion. First, the amount of time is related to the size and depth of the pores that are created on the surface. Second, a higher concentration of acid will increase the size of the pores that are created during the etching process. Overall, nitric acid dealloying is the most common process for creating nanoporous gold because it is a straightforward process that provides consistent results.

Dealloying under electrochemical control has become more common in recent years; this approach provides tighter control over the terminal porosity and ligament length. Ligament size refers to the dimensions of the regions that surround the pores on the surface of the structure. Multiple setups and etching solutions can be used to obtain the nanoporous metal structure of interest. The most popular setup for the electrochemical cell involves etching a gold-silver alloy in which the alloy surface acts as the working electrode and a noble metal (platinum, gold, silver) acts as the counter electrode. The setup also has a Ag/Ag+ reference electrode. The protocol generally applied to the cell is a constant voltage over a defined period of time. An important parameter indicative of etching is that the charge being passed through the cell is increasing at a generally linear rate. An important parameter for the etching process is the potential that is applied; one method for determining the

potential is based on the oxidizing range for the metal that needs to be removed. The metal that is being oxidized is losing electrons to the working electrode and is being deposited onto the counter electrode. The general range for silver/gold dealloying is 1-2 V. Dealloying under electrochemical control provides enhanced control over the ligament size; structures obtained using this technique may possess ligament sizes down to 10 nm (Biener 2006). In comparison, structures obtained using free corrosion may possess ligament sizes down to 25-50 nm.

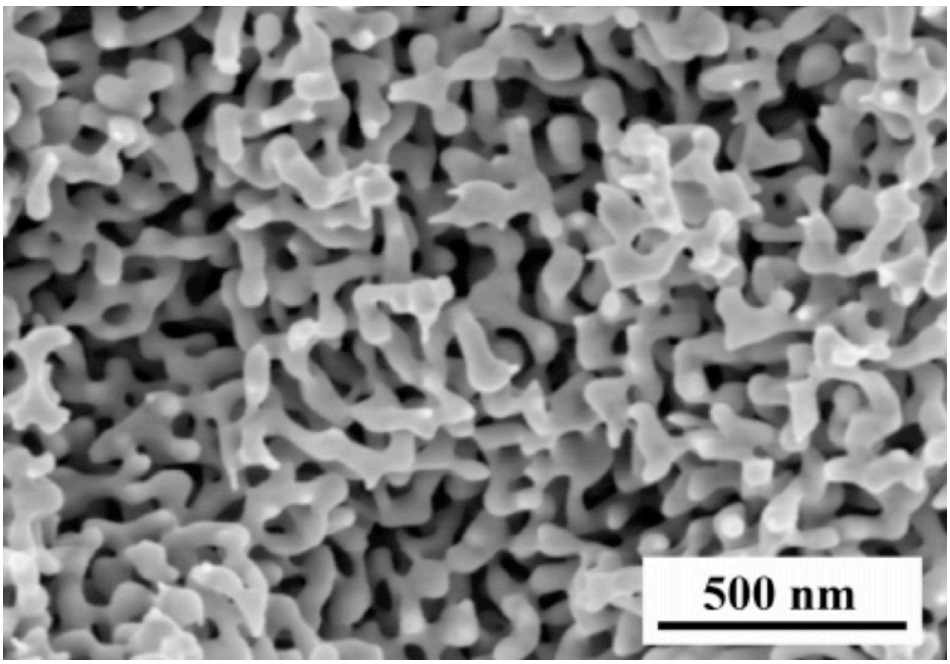

Figure 5. Scanning electron microscopy micrograph of spongelike nanoporous gold material. Reprinted with permission from Biener J, Hodge A, Hayes J, Volkert C, Zepeda-Ruiz L, Hamza A and Abraham F (2006), 'Size effects on the mechanical behavior of nanoporous Au', *Nano Letters*, 6, 2379-2382. Copyright (2006) American Chemical Society.

Snyder (2008) completed a study involving free corrosion with nitric acid and electrochemical etching. One option for the etching solution is silver nitrate (0.1 M) because silver that is removed from the alloy will deposit on the counter electrode (Snyder 2008). Ideally, the silver concentration does not dramatically change, providing consistent removal of the silver from the alloy. Perchloric acid can be used in place of nitric acid. Jin (2009) used perchloric acid as well as an electrochemical cell setup; a potential of 650 mV was applied for 17 hours. Senior (2006) applied a potential of 1.1 V over a processing time 30 seconds to an alloy sample; 0.77 M perchloric acid was used in this study. Senior (2006) also applied a potential of 1.0 V over a processing time of 120 s and applied a potential of 920 mV over a processing time of 3 hours (Senior 2006.) The combination of lower potential values and longer processing times was associated with a much more uniform gold structure. Biener (2006) showed complete removal of silver from a gold-silver alloy using a potential of 1 V and an etching solution containing 1 M HNO_3 and 0.01 M $AgNO_3$. Similarly, Gittard (2010) processed gold-silver alloy wires using an etching solution containing 1 M HNO_3 and 0.01 M $AgNO_3$ for approximately 30 minutes. The variability of the electrochemical procedures used in previous studies provides many options for future research. There are advantages and disadvantages to each electrochemical etching method; the most uniform pore size porous materials were generally created at lower potentials over longer periods of time (from many minutes to hours). It should be noted that electrochemical methods enable removal of 90-95% of the silver from the alloy. Electrochemical etching also provides an appropriate method to obtain controlled pore sizes as well as deep and long ligaments.

An alternative to using nitric acid or another type of acid for electrochemical processing involves using zinc chloride and dimethyl sulfoxide. Dong (2009) demonstrated use of DMSO/$ZnCl_2$ electrolyte for creating nanoporous gold; the addition of heat to the solution increased the speed of alloying and dealloying reactions. Post-treatment procedures using sulfuric acid were also demonstrated.

In general, nanoporous metals exhibit mechanical properties that differ from those of their continuous bulk counterparts. In particular, nanoporous gold exhibits brittle properties; these properties lie in stark contrast to the ductile nature of bulk gold (Mathur 2007). Nanoporous metals have a Young's modulus that is directly proportional to the porosity of the sample. A straightforward way to explain the relationship is to consider a sponge that is made of a metal. If material is removed from a metal sponge structure, the outer dimensions of the structure are not altered. Because of the absence of support material, it becomes more brittle and exhibits a higher Young's modulus value. This logic can also be applied to nanoporous metals. In general, a sample of nanoporous gold with a higher degree of porosity will be a weakened structure that exhibits higher yield strength and lower plastic deformation values.

Several studies have been conducted to investigate the mechanical behavior of nanoporous gold and the approaches for altering its mechanical properties. Seker (2007) investigated the effects of annealing beams, films, and cantilevers of nanoporous gold at several temperatures. Use of annealing procedures both before and after the nitric acid dealloying process was assessed; a higher annealing temperature was associated with a stiffer

material (Seker 2007). Mathur (2007) investigated the effect of ligament size on Young's modulus. This study indicated that the Young's modulus significantly decreased for materials with larger ligaments. This result was attributed to the fact that an increase in ligament size is associated with more ductile behavior and lower Young's modulus values. Overall, nanoporous gold exhibits largely brittle behavior; as such, this material must be carefully handled for use in many biomedical applications.

2. ELECTROCHEMISTRY OF NANOPOROUS MATERIALS

When a potential is applied to nanoporous gold, it exhibits a capacitor-like behavior that can be modelled and evaluated. Robinson (2010) explained this behavior using the De Levie model and showed how a porous electrode was charged with ions from the solution or discharged depending on the potential that was applied to the electrode. To examine this model, nanoporous wires were created through electrochemical etching; a cyclic voltammogram was subsequently obtained from gold nanoporous electrodes in a solution of 1 M perchloric acid.

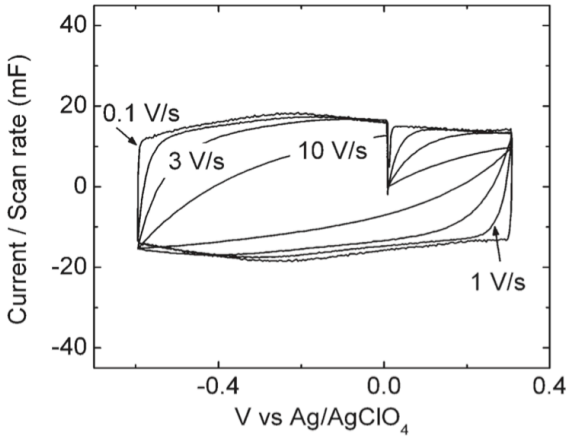

Figure 6. Cyclic voltammograms for a nanoporous gold electrode in 1 M perchloric acid. Reprinted (adapted) with permission from (Robinson D, Wu C, Ong M, Jacobs B, Pierson B (2010), 'Effect of electrolyte and absorbates on charging rates in mesoporous gold electrodes', *Langmuir*, 26, 6797-6803.). Copyright (2010) American Chemical Society.

The capacitance of the wire can be derived from a cyclic voltammogram and the wire geometry. The equation that models the capacitance using the characteristics of the normal, non-porous gold material is as follows:

$$C_{wire} = \left(2\Pi r_w^2 L_w P C_{dl}\right)/r$$

C_{wire} is the capacitance of the wire
r_w is the wire radius
L_w is the length of the wire
P is the porosity parameter
C_{dl} is the planar capacitance per unit area of the material used
r is the radius of the pores

The experimental capacitance from the wires used by Robinson (2008) was about 15 mF based on the observed plot in Figure 6; the expected value was 12 mF. The capacitance of non-porous gold has been observed to be between 1-2 μF and the expected value from the

equations is 2 μF (Robinson 2010). The capacitive behavior of nanoporous gold enables it to be used in a variety of medical applications.

3. GOLD AND SILVER THIN FILMS

Thin films of metal alloys are important and interesting field. Metals can be applied to a number of surfaces with silicon providing a good medium because of its electrical conductance as well as its ability to act as the basis for crystal growth during processes such as pulsed laser deposition (PLD). By using a laser to ablate material onto a substrate, a film of precise thickness and composition can be created (Ganeev 2007). The normal method for producing the thin films of PLD is to do the ablation in a vacuum environment to encourage the formation of the film on the opposing substrate instead of the material simply redepositing onto the target material (Ganeev 2007). The creation of nanoparticles along with thin films on surface of the substrate can be seen in Figure 7. The work completed at North Carolina State University in conjunction with the Materials Science and Engineering Department will be aimed at creating thin films with textured surfaces and even film growth on the surface of the silicon substrates used.

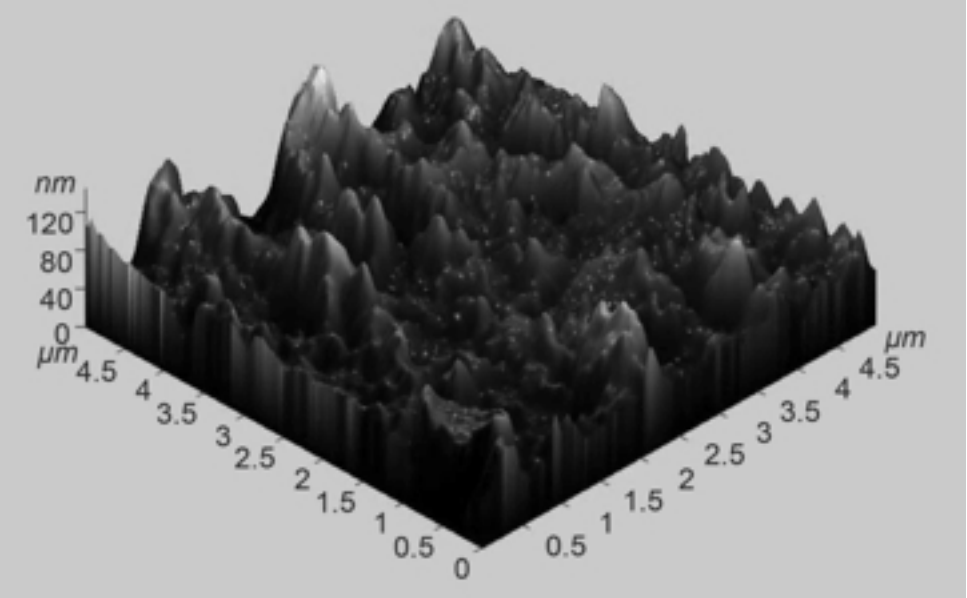

Figure 7. Atomic Force Microscopy image of the Ag nanoparticles deposited on a Cu strip in tight-focusing conditions. Ganeev R, Chakravarty U, Naik P, Srivastava H, Mukherjee C, Tiwari M, Nandedkar R and Gupta P (2007), 'Pulsed laser deposition of metal films and nanoparticles in vacuum using subnanosecond laser pulses', *Applied Optics*, 46, 1205-1210.

4. ANTIMICROBIAL ACTIVITY OF SILVER AND GOLD

Antimicrobial activity of silver and gold has been well documented in the past. The application of the metals in an alloy arrangement is an important area to discuss. Because neither gold or silver easily oxidizes, the metals can exist in harsh environments such as *in vivo* with medical devices. Past work by Reddy has shown that (2012) nanoscale particles of gold and silver can have a profound antimicrobial effect. The application of antimicrobial silver is widely known and detailed in previous work by Dr. Roger Narayan in polymer and

other applications. The application of thin film silver and gold alloys will provide a new understanding of the antimicrobial effects the metals exhibit. In addition,using the nanoporous materials of a silver and gold alloy should show antimicrobial effects consistent with other work. Reddy showed significant antimicrobial activity by using hydrogels impregnated with silver and gold nanoparticles (2012). The results from their work showed that their hydrogel contained silver and gold throughout the gel and it was able to have significant effect of inhibiting bacteria growth through disk diffusion testing (Reddy 2012). As seen in Figure 8, the hydrogel samples have a clear zone of inhibition compared to the control.

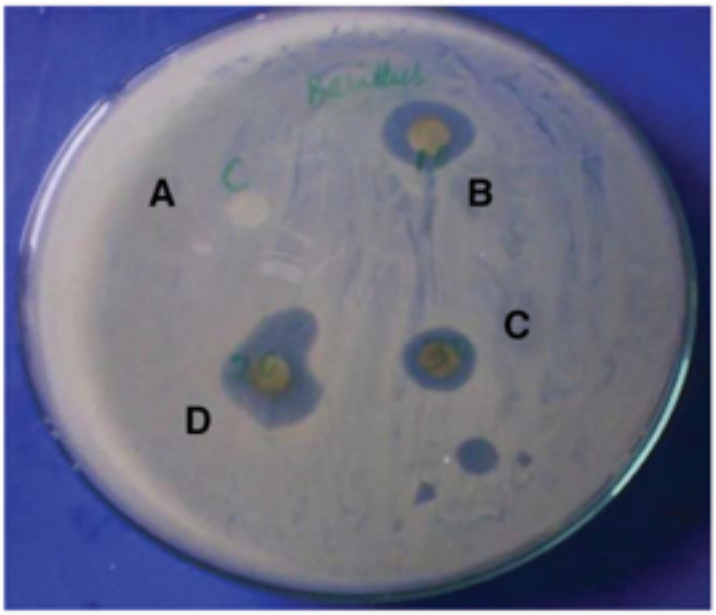

Figure 8. Antibacterial activity of (A) blank hydrogel, (B) Ag nanocomposite hydrogel, (C) Au nanocomposite hydrogel, (D) Au with Ag nanocomposite hydrogel. Reddy P, Varaprasad K, Narayana N, Raju K and Reddy N (2012), 'Fabrication of Au and Ag Bi-Metallic Nanocomposite for Antimicrobial Applications', *Journal of Applied Polymer Science*, online.

Nanoporous gold is a material that can be utilized in several areas of medical research, including biosensing and drug delivery. The precursor alloy can be designed with formulations of gold and silver that provide optimized electronic and mechanical properties. Due to its brittle nature, nanoporous gold has been restricted in use as an electrode material in biosensors, drug delivery devices, and other applications. Processes such as annealing have been shown to produce a tougher and less brittle material. Optimizing mechanical properties of nanoporous gold is necessary to enable its use in a wider variety of medical applications.

III. EXPERIMENTAL

2. BIOMATERIAL PRODUCTION

3. ETCHING PROCESS FOR WIRES

Nanoporous materials can be produced in a number of ways that were described in the background section. In order to create a nanoporous wire with repeatable properties and a controlled amount of silver remaining, electrochemically controlled etching is a ideal method. In order to create the nanoporous structure and selectively remove silver from the gold and silver alloy wires, both an acid solution and an electrochemical cell is needed.

The wires that are used for the etching process are extremely precise alloys produced by Refining Systems Inc. from Las Vegas, Nevada. The wires were purchased as 50 % Ag 50 % Au by weight in a diameter of 0.2 mm. The wires were then cut with a razor blade to each be 4 cm long. Finally, a 0.2 mm 99.9 % Au wire, also from Refining Systems Inc., is wrapped around the wire to create a structural support for the alloy wire.

The electrochemical cell used for the etching process can be seen in Figure 7 and is composed of a glass beaker, acrylic electrode holder and three electrodes. The black connector attaches to a 99.9% Au wire that is used as the counter electrode. The red connector is the working electrode and is attached to the top of the Au wire wrapped around the silver/gold alloy wire. The yellow connector is attached to a Ag/Ag^{+} reference electrode from Bioanalytical Systems Inc. The cell is composed of a glass beaker and an acrylic electrode holder shown in Figure 9. The solution used for etching the wires was an acidic solution composed of 1M nitric acid and 10mM silver nitrate.

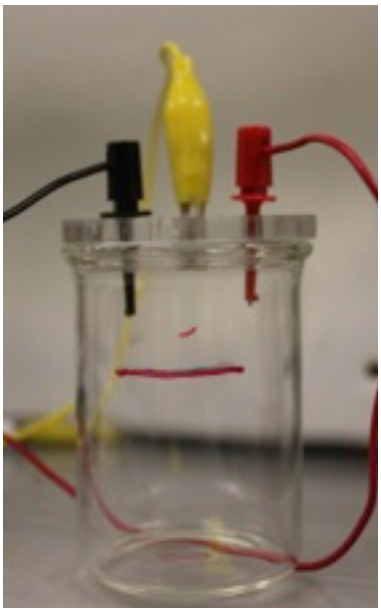

Figure 9. Image of the electrochemical cell with three electrodes, glass beaker and acrylic electrode holder.

The electrochemical cell is controlled by a Princeton Applied Research 273A potentiostat/galvanostat that was connected to a PC using a National Instruments GPIB to USB converter cable. The PC controlled the potentiostat with a LabVIEW program written by Dr. David Robinson for etching the wire and monitoring the total amount of charge that was passed through the wire during the etch.

The procedure for etching the wires involved two steps. The first step was to place the alloy wire into the 1M nitric acid solution and run a CV on the wire to double check the wire and make sure that everything is connected correctly. The Pre-Etch CV was ran as follows:

V_1 = 0 mV
V_2 = -1500 mV
V_3 = 0 mV
Scan Rate = 50 mV/s
Current Range = 100 nA/V
Pre-delay = 5 seconds

Once the Pre-Etch CV was complete, then the Charge Monitor program was loaded and the etch process would begin. The Charge Monitor program was run in the following method for each wire. The only difference between wires was the stopping point for the process based on the total charge passed through the system. In previous work, the Charge Monitor program was run until at least 7.5 Coulombs (C) had passed. The general range was 7.5-10 Coulombs. In this testing, the wires were etched until the program determined that the following amounts of charge had passed through the wires: 2.5 C, 3.75 C, 5 C, 6.25 C, 7.5 C. Two wires were etched at each of the five levels for a total of 10 etched wires. TM3 and TM6 were disregarded due to incomplete processing during the etch and TM11 and TM12 replaced them in the set of wires. The parameters for the etch process are detailed below:

Bias = 1000 mV
Iterations = 4000
Interval = 1 second
Current Range = 10 μA/V

Once the wires were complete and the etch process had finished, the wires were rinsed with deionized water and placed into a glass vial containing more deionized water to soak for at least 24 hours in order to allow all the etching process chemicals and residues to be removed from the wires.

4. CHARACTERIZATION FOR WIRES

In order to determine the electrochemical properties of the etched alloy wires, each wire was characterized using an electrolyte solution of 0.5M sodium trifluoroacetate. In table 1, the results from the characterization process can be found. The electrochemical method used to characterize the wires was a CV. The electrochemical cell used was the same as the etching process except for two changes. The reference electrode used was a Ag/AgCl reference electrode and the counter electrode was platinum mesh. The beaker was filled with the electrolyte solution of sodium trifluoroacetate. Sodium trifluoroacetate was used because of the relatively equal charge mobility of the sodium and TFA molecules. Once the cell was set up appropriately, the LabVIEW CV program, again designed by Dr. David Robinson, was loaded and the CV was applied to the wire in order to determine the response. The characterization of the wires used the protocol described below. The only difference between wires was the scan rate and current range as that depended on each wires porosity.

V_1 = 300 mV
V_2 = 600 mV
V_3 = 0 mV
Scan Rate = 1 - 25 mV/s
Current Range = 100 nA - 1 mA/V
Pre-delay = 15 seconds

The results from the CV process was a text file that was imported into Excel and then plotted using Origin 8.5 in order to visualize the data. The measurement for the capacitance of the wire is described below using electrical properties. The capacitance measurement uses the relationship of the charge present of the surface of an electrode:

$$q = CE$$

q = charge in Coulombs; C = capacitance in Farads; E = potential in Volts.

Integrating with respect to time the formula changes to:

$$dq/dt = C\ dE/dt$$

Note that $dq/dt = i$ *(Current)* and $dE/dt = v$ *(Scan Rate)*.

Thus, the calculation to find the capacitance of the wire from the CV was:

$$C = i / v$$

$$C = ((i_1 - i_2)/2)/v$$

The calculations were made at 150 mV and 450 mV using the average current value at each potential. i_1 and i_2 were measured at the same potential on the plot.

5. PULSED LASER DEPOSITION

The thin film alloy samples were prepared using a method called pulsed laser deposition (PLD). PLD is a method used in many areas and in this project it was chosen to produce very thin films on silicon wafer substrates from an alloy target. PLD uses an excimer laser to ablate a target material onto a substrate material in a vacuum chamber. As seen in Figure 8, the target material is placed on a rotating platform that ensures the laser interacts with a wide ranging portion of the target. The laser energy vaporizes the target material in the chamber and deposits the vapor onto the substrate material. The target material used for this PLD was also from Refining Systems Inc. and was in the following compositions:

Percentages of AgAu by weight:
1 x 99.9% Ag
1x 90/10 % AgAu
1 x 75/25 % AgAu
1 x 50/50 % AgAu
Diameter 20 mm
Thickness 2 mm

The substrate material was prepared from 10 cm diameter silicon wafers and etched using a diamond scribe into rectangular sections that were approximately 1 cm by 1 cm. The silicon substrates were then cleaned by placing them into an acetone bath at 200°C for 10 minutes. The silicon substrates were loaded into the vacuum chamber using conductive silver paste onto the sample holder. The vacuum chamber was then lowered to the desired pressure and the samples were created. The protocol for creating the samples is listed below:

Laser: Lambda Physik LPX200 KrF excimer laser with $\lambda = 248$ nm and $\tau = 25$ ns
Pulse Energy: 300 mJ
Starting Angle: 43°
Ending Angle: 57°
Pulse Frequency: 10 Hz
Number of Pulses: 27,000
Vacuum Pressure: 5×10^{-6} Torr
Temperature: Room, 72°

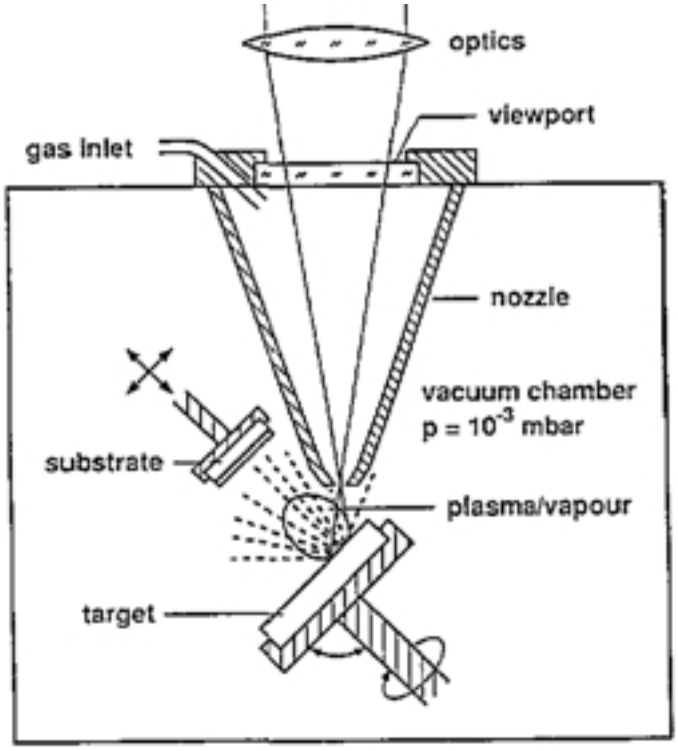

Figure 10. PLD setup using a laser and vacuum chamber. Aden M, Kreutz and Voss A (1993), 'Laser-induced plasma formation during pulsed laser deposition', *Journal of Physics D: Applied Physics*, 26, 1545-1553.

Overall, 10 silicon substrates were used for each target for a total of 40 1 cm x 1 cm samples produced using the PLD protocol.

3. TESTING OF BIOMATERIAL PROPERTIES

3. PROFILOMETRY

The PLD sample thickness was determined by using a profilometer in the Analytical

Instrumentation Facility (AIF) in the Monteith Research building on NCSU's campus. Fred Stevie measured a masked PLD sample in two places to determine the average step height. The masked region was created by placing an extra silicon wafer section that covered one corner of the silicon substrate during the PLD process. The profilometer is a Tencor P-20 with a diamond stylus, 2 μm tip radius, 10 nm horizontal resolution, vertical linearity 1 nm or 0.5%, and repeatability of 1 nm.

4. X-RAY DIFFRACTION SPECTROSCOPY

The PLD samples were analyzed to determine the crystallinity and the orientation of the film. X-ray diffraction spectroscopy (XRD) was used in EBI in the Department of Material Science and Engineering at North Carolina State University. The XRD process involves placing the samples in a chamber where a beam of intense X-rays bombard the sample as it is slowly turned to allow for the x-rays to interact with the complete sample. The resulting diffraction pattern is detected and the computer system outputs a spectrum with peaks corresponding to large concentrations of that specific crystal type.

5. ENERGY DISPERSIVE X-RAY SPECTROSCOPY

Energy dispersive X-ray spectroscopy (EDS) is a technique used to determine the exact elemental makeup of the sample. By directing an electron beam onto the sample, X-rays are released specific to each element in the sample. Those X-rays are registered by the detector and the elemental signature can be determined. The first step is to use a standard material so that the software on the EDS can more accurately determine the exact composition of the sample. For this testing, a 50/50 % by weight AgAu alloy from Refining

Systems Inc. was used as the standard. That wire is the same wire that is the precursor used in the etching process for the wires used in the rest of the testing. The EDS was part of a Hitachi S3200 Variable Pressure SEM located in the Analytical Instrumentation Facility in the Monteith Research Center at North Carolina State University.

4. SCANNING ELECTRON MICROSCOPY

For both the wires and the thin film samples, it was important to determine exactly what the surfaces of the materials looked like under high magnification microscopy. In order to get images at the level of 200,000x, the Focused Ion Beam (FIB) instrument in the AIF at NCSU was used. The FIB is a FEI Quanta 3D FEG DualBeam instrument with terrific resolution and the ability to image the pores of the wires on the scale of 50 nm. The process for getting the images involved placing the samples on a stage and working with the staff of the AIF to get the proper images. Priority was put on getting images of the pores if possible and to show the samples at a range of magnifications.

5. DISK DIFFUSION

In order to determine the antimicrobial activity of the thin film samples and the etched wires, the Kirby-Bauer disk diffusion protocol was followed with E. coli and S. aureus bacteria. *Escherichia coli* (a gram-negative bacteria strain) and *Staphylococcus aureus* (a gram-positive bacteria strain) are common to antimicrobial testing procedures and were used in disk diffusion protocol.

The Kirby-Bauer protocol is a well documented process for determining the antimicrobial activity of a sample. The process involves growing bacteria, plating the

bacteria and the sample, incubating and then imaging the agar plates. The first step is to grow the bacteria for 24 hours to allow for proliferation. The bacteria solution was then isolated and plated on Tryptic Soy Agar plates and incubated for 24 hours. The wires and thin film samples were then sterilized in a UV hood for 20 minutes. A mixture of bacteria and sterile water was then created with a turbidity comparable to a 0.5 McFarland Standard. This turbidity corresponds to a concentration of 1.5×10^8 Colony Forming Units (CFU)/mL. Once bacteria and sterile deionized water was then used to plate the bacteria onto Mueller Hinton II agar plates. After thoroughly plating the bacteria samples with three different applications with a sterile cotton applicator, the samples were plated onto the agar surface with the antimicrobial side facing the agar surface or with the maximum surface area of the wire interacting with the agar. The samples were then incubated at 37°C in 5% CO_2 in a standard biological incubator for 24 hours.

The processing of the samples involved imaging each sample with a Leica EZ4D dissection microscope. Each image set for each plate was calibrated using a transparent ruler. An image was taken for for each side of the thin film samples and each section of the wires. The measurements taken for the data for the disk diffusion involved using xScope software to measure the calibrated distance and then to measure the distance of the zone of inhibition. The distances were measured in two ways for the thin film samples and for the wires. The thin film samples were measure three times per side by splitting up the face into three regions. The maximum perpendicular distance of an absence of bacteria was the distance

recorded for each side. The wire measurements were similar and instead of using three measurements, four were taken on top of the wire and four on the bottom of the wire. The reasoning for this was that the wires required at least four images to capture the entire length of the wire. The data was then averaged and analyzed for entire sample.

IV. RESULTS AND DISCUSSION

4. WIRE TESTING RESULTS

4. ELECTROCHEMICAL PROPERTIES

The wires that were etched to create nanoporous materials showed a wide range of electrochemical properties. Wires TM1, TM2, and TM4 exhibited a resistor like response in the CV in the sodium trifluoroacetate. These wires had very low capacitance and did not store as many electrolytes as the other wires. The CV response curve can be seen for TM2 in the left of Figure 11. The maximum capacitance for that group of wires was 0.32 μF in TM2. The CVs of TM1 and TM4 can be located in the Appendix and exhibit no discernible capacitive nature in their response curves.

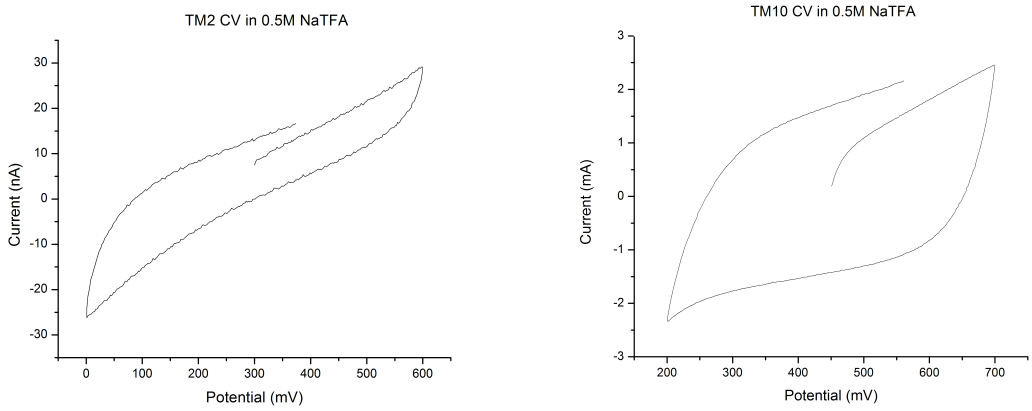

Figure 5. Cyclic voltammogram plots of wires TM2 and TM10 in 0.5M sodium trifluoroacetate electrolyte solution.

The next set of wires that had similar properties were TM11, TM5, TM12, TM7, TM8, TM9, and TM10. The CV response curves for these wires was much more capacitive in shape and showed a significant amount of stored charge over the scan with the potentiostat. The average of 22.68 mF at 150 mV and 24.68 mF at 450 mV showed a significant amount of stored sodium trifluoroacetate on the wires. The data was extremely variable though, with a very large standard deviation for both measurements. The likely reason for this variability is inherent to the etching process with electrochemical control. Each wire was etched in a similar fashion with the only difference between them the amount of time and total charge that was passed through the wires. The normal capacitance for a non-etched wire is around 1-2 μF (Robinson Shaun) so the results from the second set of wires showed a significant increase in capacitance compared to a normal alloy wire. TM10 showed an extremely favorable results at two different potential sweeps. In Figure 5, the tilted box shape of the CV response curve is the ideal result from a supercapacitive wire. TM9 and TM10 were analyzed at different potential ranges with their results in Table 1 signified by **. The reason for altering the potential ranges was to maximize the capacitive behavior of the wire.

Table 1. Capacitance Measurement from the characterization of etched gold/silver alloy wires in 0.5M sodium trifluoroacetate.

Capacitance Measurement (300mV, 600mV, 0mV)	**At 150 mV**	**At 450 mV**
TM1	0 μF	0 μF
TM2	0.32 μF	0.19 μF
TM11	0.86 mF	0.87 mF
TM4	0.01 μF	0.02 μF
TM5	30.04 mF	10.64 mF
TM12	1.28 mF	1.08 mF
TM7	5.4 mF	4.28 mF
TM8	30.2 mF	41.3 mF
TM9	34.2 mF	71.8 mF
TM10	56.8 mF	42.8 mF
**TM9 (300mV, 600mV, 150mV)	101.5 mF	123.5 mF
**TM10 (450mV, 700mV, 200mV)	150.5 mF	160 mF
Average: TM1, TM2, TM4	0.11 μF ± 0.18	0.07 μF ± 0.10
Average: TM11, TM5, TM12, TM7, TM8, TM9, TM10	22.68 mF ± 20.98	24.68 mF ± 27.57

2. THIN FILM TESTING RESULTS

1. PROFILOMETRY

After completing the PLD process on the masked sample with 600 pulses and 10 pulses per second, the measured thickness was an average of 30 nm. All of the PLD samples were then processed at rate of 10 pulses per second with 2700 pulses. PLD is understood to be a linear process, so the thickness of the PLD samples tested are approximately 30 nm x (2700/600) = 135 nm.

2. X-RAY DIFFRACTION

All peaks seen in the XRD patterns of the targets belong to Ag. This shows that the targets are uniform and ideal solid solutions of Ag and Au. This suggestion is confirmed by the peak broadening when Au is added to Ag. The XRD patterns of the samples indicates that the films have a textured or epitaxial structured, since they have mostly assumed a 111 direction. The growth of the thin films in a textured format is also confirmed by the SEM images from the previous section. The peak shift has its origin in in-plane strain due to incorporation of gold to silver.

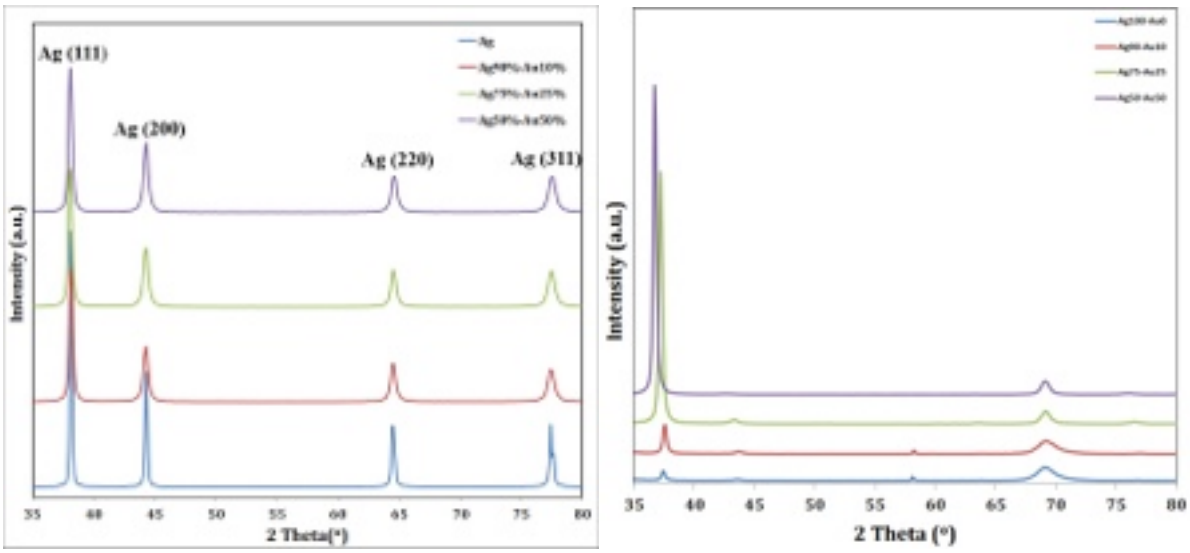

Figure 12. X-ray diffraction spectroscopy of the PLD targets (left) and produced PLD samples (right).

3. COMBINED TESTING RESULTS

1. ENERGY DISPERSIVE X-RAY SPECTROSCOPY

After the wires have been etched to create the nanoporous structures by removing silver from the alloy, the wires were tested using spectroscopy and electrochemical methods to determine the porosity and the electrochemical properties. Using energy dispersive X-ray spectroscopy (EDS), the specific components of the sample can be determined in a weight percentage. The goal of the etching process was to create a range of wires with different amounts of silver remaining in the wire in order to increase the antimicrobial properties of the wire. As seen in Table 2, the wires were etched to different total charge amounts from 2.51 Coulombs to 7.54 Coulombs. The range of the silver remaining in the samples was from

11.23 wt. % - 19.13 wt. % Ag. During previous testing and documented research from our lab in conjunction with Dr. David Robinson's lab, the average remaining silver was 5 wt. % Ag (Robinson Gittard). The additional silver in the wires was intentional and will be discussed further in the antimicrobial testing results. The etching process to different charge levels was not successful in creating distinctly different quantities of remaining silver.

Table 2. Energy dispersive X-ray spectroscopy for nanoporous wires.

Sample Name	Ag Weight %	Au Weight %	Total Charge Etched (Coulombs)
TM1	19.13 ± 0.92	80.97 ± 1.83	2.51
TM2	14.85 ± 0.91	85.15 ± 2.16	3.01
TM11	13.13 ± 0.83	86.87 ± 2.18	3.77
TM4	19.01 ± 0.92	80.99 ± 1.84	3.75
TM5	12.24 ± 0.70	87.76 ± 1.99	5.03
TM12	11.23 ± 0.75	88.77 ± 2.22	5.47
TM7	n/a	n/a	6.26
TM8	11.23 ± 0.65	88.77 ± 2.00	6.55
TM9	12.46 ± 0.81	87.54 ± 2.21	7.53
TM10	13.63 ± 0.75	86.37 ± 1.95	7.54

The Ag wt. percentages with the highest amount of remaining silver, TM1, TM2 and TM4, did show an interesting correlation to the capacitance of those wires. It can be deduced

that because there was a higher percentage of silver remaining in the wire, the wire was less porous and thus had a smaller amount of possible surface area to charge during the CV process. The EDS process also showed that the samples were free of any impurities or contamination. Figure 13 shows the EDS spectrum of TM1 which was characteristic of the other samples processed through etching.

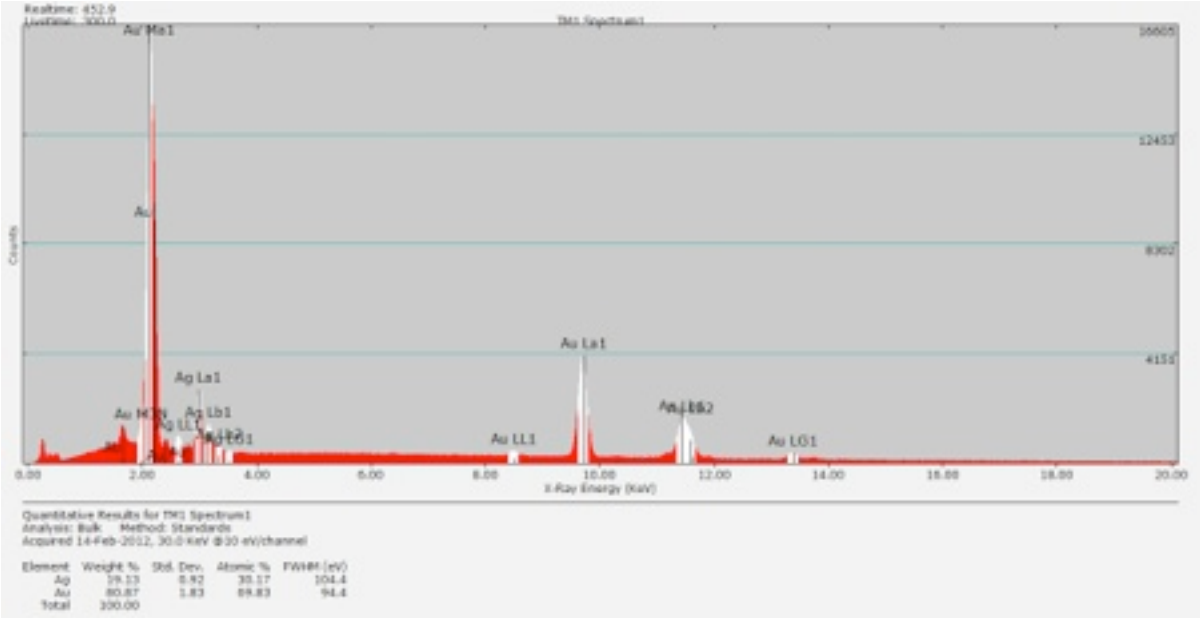

Figure 13. EDS spectrum of wire TM1.

Table 2. Energy dispersive X-ray spectroscopy for thin film pulsed laser deposition samples.

Sample Name	Ag Weight %	Au Weight %
Targets		
50Ag/50Au wt%	51.25 ± 1.39	48.75 ± 1.19
75Ag/25Au wt%	74.36 ± 1.94	25.64 ± 1.04
90Ag/10Au wt%	89.29 ± 2.27	10.71 ± 0.63
99.9Ag wt%	n/a	n/a
PLD Samples		
50Ag/50Au wt%	31.61 ± 1.23	68.39 ± 1.67
75Ag/25Au wt%	77.34 ± 2.09	22.66 ± 1.02
90Ag/10Au wt%	84.07 ± 2.23	15.93 ± 0.84
99.9Ag wt%	100.00 ± 2.66	n/a

The PLD samples and the PLD targets were tested using EDS as well to confirm the compositions of each. The targets used in the PLD process were very accurate to their stated compositions with little deviation as seen in Table 2. The PLD samples used the target material to deposit onto silicon wafer substrates. EDS was used to confirm the composition of the PLD samples. The 50/50 % AgAu sample was determined to have 32/68 AgAu % which was not ideal and likely a result of the variability inherent to PLD and the high percentage of Au that can be a difficult metal to deposit consistently.

2. SCANNING ELECTRON MICROSCOPY

Both the wires and the PLD thin film samples were imaged using SEM in order to confirm the uniformity and/or porosity of the sample types. Figure 14 shows the surfaces of the PLD samples as uniform and consistent depositions on the surface of the silicon wafers. The dimpled surface is characteristic of PLD applied thin films and shows consistency across the samples. The top left image shows the 50/50 % AgAu sample at 1000x to show the macro surface. The small pin holes are also expected for a PLD thin film. There is a small scratch on the 1000x image, and that could impact the surface integrity of the samples. PLD applied thin films at 135 nm thick can be easier disturbed or scratched off.

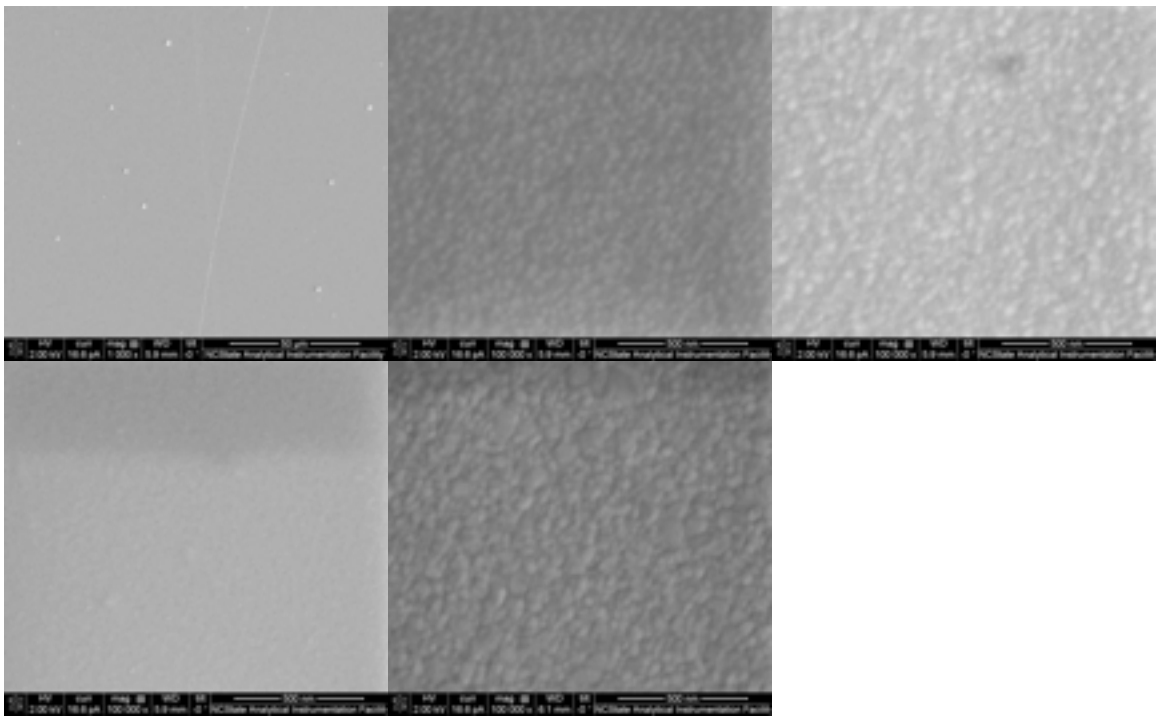

Figure 14. SEM images of PLD samples (left to right, from top left) at 100,000x. 50/50 % AgAu PLD (1000x), 50/50 % AgAu PLD, 75/25 AgAu % PLD, 90/10 AgAu % PLD, 99.9 Ag % PLD.

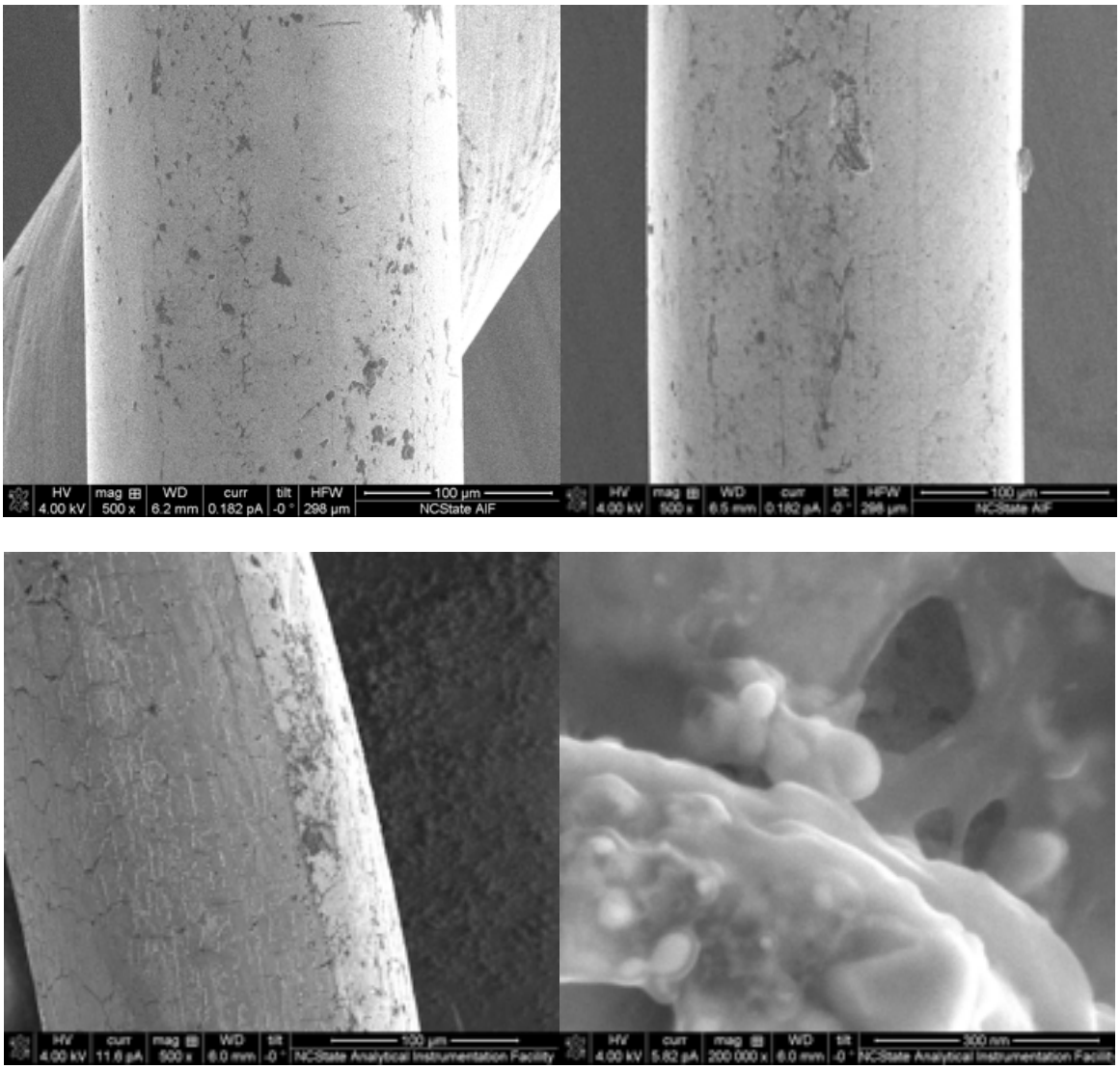

Figure 15. SEM images of alloy wires before and after etching (left to right, from top left): 50/50 % AgAu braided at 500x, 50/50 % AgAu at 500x, TM1 at 500x, TM1 pores at 200,000x.

The wires imaged with the FEI SEM provided interesting and important data for surface characteristics. Figure 15 shows two wires at two different magnifications: 50/50 % AgAu non-etched wire and TM1. The first image depicts the braided alloy wire with a 99.9%

Au wire wrapped around the 50/50 % AgAu wire. The surface of the wire shows some pitting and other deformities, but the wire is not cracked or missing large sections. The bottom left image, TM1 at 500x, shows large scale cracking and distinct grain boundaries. The image also shows material on the edge of the grain boundaries which is hypothesized to be silver that has been brought to the surface of the wire. The bottom right image shows the pores of TM1 at 200,000x. The pores in this image were measured to range from 71.01-433.53 nm. Overall, six of the ten wires had images clear enough to measure the pores in the images. The average size of the pores was calculated to be 117.22 nm. The expected pore size was much smaller on the order of 10-20 nm because of previous work from labs of Dr. David Robinson. The likely reason for the larger pores was the truncated etching process that deliberately left excess silver in the pores. If the wires had been etched to completion, to around 10 Coulombs, the pore sizes most likely would have been much smaller and more prevalent.

Table 3. Pore sizes measured from SEM images.

Sample Name	Pore 1 (nm)	Pore 2 (nm)	Pore 3 (nm)
TM1	153.62	71.01	433.53
TM2	117.83	57.83	85.30
TM12	115.61	57.80	170.52
TM7	199.42	124.28	137.28
TM8	28.90	65.03	180.64
TM10	26.01	46.24	39.02
		Average:	**117.22**

3. ANTIMICROBIAL ACTIVITY

The results from the Kirby-Bauer disk diffusion test showed impressive antimicrobial activity from the etched wires. The thin film samples showed minimal impact except for the highest silver concentration samples. Examining the E. coli samples first, Figure 16 shows the images from the testing with the controls and the gold/silver samples. The normal method for testing disk diffusion is to use circular or rectangular samples for easier measuring. The PLD samples showed minimal effect but the 99.9% Ag PLD sample an impressive response. The zone of inhibition ranged from 0 mm to 1.5 mm, increasing with the percentage of silver in the thin film. This confirms the hypothesis that increasing the amount of silver will indeed increase the antimicrobial effect. The wires showed significantly more activity with all samples providing an average of 4.2 mm of inhibition and a maximum of 4.9 mm average

zone for TM9. The reason that the thin films did not have a greater impact was the composition and structure of the film. The thin films were not water soluble so it was difficult for the silver to migrate from the surface of the film. Also, because the films were relatively thin, 135 nm, there was significantly less material than the wires. The wires had an impressive impact mainly because of their ability to diffuse silver ions from the inner surface areas of the porous regions. Upon investigation of the 35x image of TM1, there are distinct bands of material that has leached out of the wire. The assumption should be made that that material is either gold or silver because the EDS results depict no impurities in the samples. Further investigation into the composition and source of the leached material is needed to confirm this assumption.

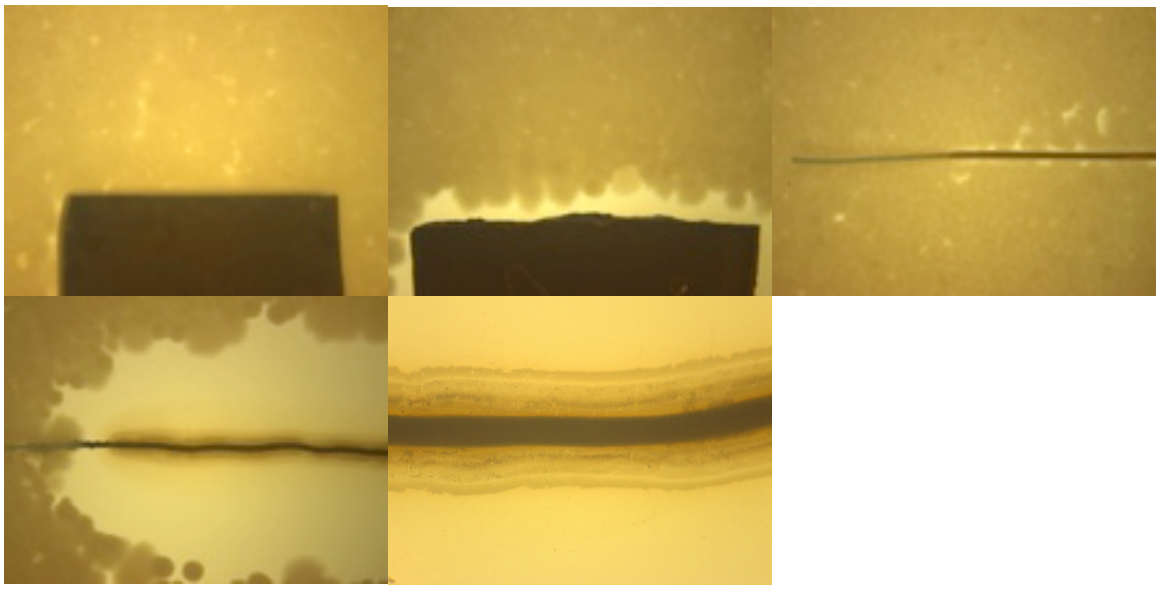

Figure 16. E. coli disk diffusion. (left to right, from top left): silicon control, 99.9% Ag PLD, 50/50 % AgAu control wire, TM4, TM1 at 35x.

The S. aureus samples and wires exhibited a very similar response to the bacterial in the test. From the images in Figure 8, the S. aureus bacteria appears to be much more confluent and grew more evenly than the E. coli samples. The average zone of inhibition for the S. aureus PLD samples ranged from 0 mm to 0.8 mm. The S. aureus samples also increased the effectiveness directly with an increased amount of silver in the film. The S. aureus wires showed an equally impressive average zone of inhibition ranging from 3.7 mm to 4.8 mm with the largest zone belonging to TM12. The same assumptions can be made about the S. aureusS. aureus wire results as the E. coli wires.

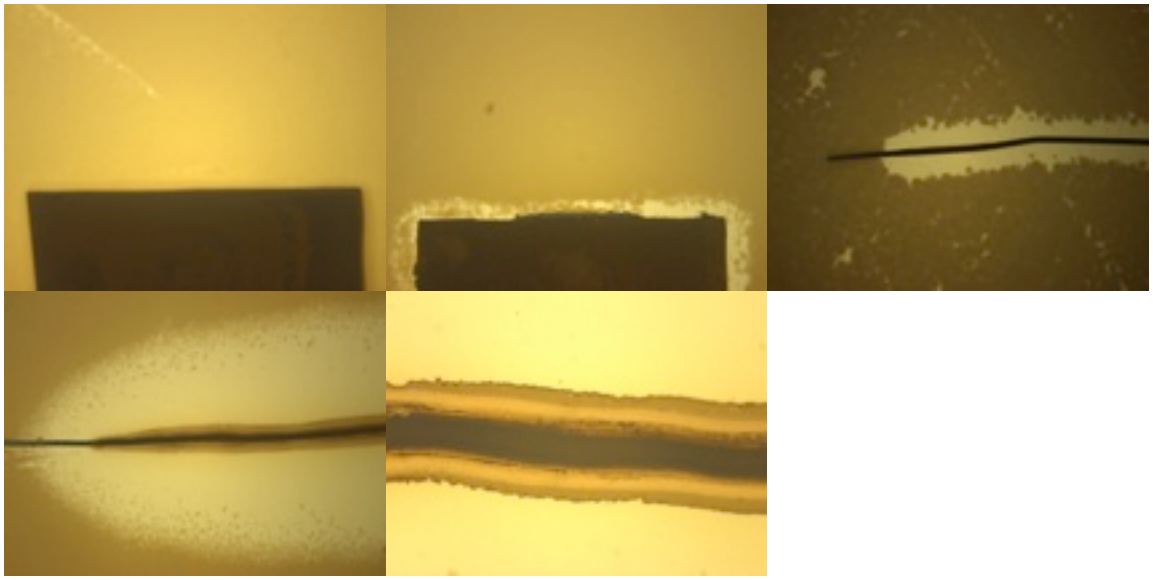

Figure 17. S. aureus disk diffusion. (left to right, from top left): silicon control, 99.9% Ag PLD, 50/50 % AgAu control wire, TM10, TM2 at 35x.

An important comparison for both the E. coli and S. aureus wires exists between the etched and non-etched wires. The E. coli 50/50 % AgAu wire exhibited a very small zone of

inhibition at 0.1 mm. This is most likely due to operator error when plating the sample as the wires were only effective where they were touching the surface of the agar plate. Increasing the sample size to include an n=3 or more would be needed to confirm that small of an effect on the bacterial growth. The S. aureus 50/50 % AgAu wire showed a more impressive effect at 1.0 mm but was still not nearly as effective as the least effective etched wire, TM8, at 3.7 mm. This direct comparison of etched vs. non-etched wires shows that because the wires were porous and contained silver that was much easier to diffuse into the agar, etching the silver/gold alloy wire produces an antimicrobial activity increase of 3.7-4.8 x the zone of inhibition of a normal non-etched wire. The complete results from the disk diffusion test for both bacteria strains can be found below in Table 6.

Table 5. Disk diffusion results for E. coli and S. aureus PLD thin films and alloy wires.

E. coli	Average Zone of Inhibition (mm)		S. aureus	Average Zone of Inhibition (mm)
Si Control	0.0 ± 0.1		Si Control	0.0 ± 0.0
50/50 % AgAu PLD	0.8 ± 0.3		50/50 % AgAu PLD	0.2 ± 0.2
75/25 % AgAu PLD	1.0 ± 0.5		75/25 % AgAu PLD	0.0 ± 0.0
90/10 % AgAu PLD	1.3 ± 0.1		90/10 % AgAu PLD	0.5 ± 0.1
99.9 % Ag PLD	1.5 ± 0.3		99.9 % Ag PLD	0.8 ± 0.1
50/50 % AgAu I Wire	0.1 ± 0.2		50/50 % AgAu II Wire	1.0 ± 0.2
99.9 % Au I Wire	0.7 ± 0.4		99.9 % Au II Wire	0.3 ± 0.1
TM1	4.2 ± 0.8		TM2	4.2 ± 0.5
TM4	4.8 ± 0.4		TM11	4.4 ± 0.4
TM5	4.1 ± 0.7		TM12	4.8 ± 0.2
TM7	4.2 ± 0.4		TM8	3.7 ± 0.9
TM9	4.9 ± 0.9		TM10	4.3 ± 0.4

V. CONCLUSION

The results from the testing accomplished for this work were used to answer the hypothesis:

Nanoporous gold and silver alloys in both thin films and electrochemically produced wires exhibit electrical properties for drug delivery as well as antimicrobial activity that would prove beneficial for use in medical applications.

In order to answer the hypothesis, objectives were the basis for the testing and analysis.

- *Electrochemically produce nanoporous metal alloys with gold and residual silver content*

In past work, the objective for nanoporous wire creation was to remove the maximum amount of silver in order to increase the porosity and capacitive nature of the wire. The experiments for this work were designed to retain the porous and capacitive nature of the nanoporous wires while also retaining a greater percentage of silver content. The EDS data showed that the wires produced using the modified procedures detailed in the experimental section retained 11-19% Ag by weight. This data showed the ideal percentages of silver were retained through the testing. The previous testing showed silver retained was around 5% Ag by weight. The increased silver content was the goal of this testing and was achieved.

Although silver was retained in the wires, the correlation between charge volume during the etch and silver content was not present. Future work for production of the

nanoporous wires should be centered around a tighter control over the outcome of the silver content. Possible methods for better control over the silver content would be to change the bias, or potential, applied to the electrochemical cell. All of the testing reported here was based on changing the total charge passed through the wire. Another possible method for creating more controllable residual silver contents would be to start with different alloys of differing amounts of silver. All of the wires produced for this testing used 50/50 % AgAu by weight.

- *Electrochemically characterize the nanoporous alloys for drug delivery applications as well as show antimicrobial action greater than non-porous materials*

Using SEM, the wires also were determined to have surface geometries with pores on the average size of 111 nm. In order to confirm the surface images with analytical data, CVs were run on the wires that showed supercapacitive behavior with extremely impressive capacitance measurements. The wires that had the greatest amount of porosity were the wires with the most silver removed during the etching process. Those wires also showed significantly more capacitance than the wires with more residual silver. Although the wires showed an impressive amount of capacitance, the results were not conclusive because the variability in the data was large. The main reason for the large variability was linked to the inability to produce wires with an expected amount of residual silver.

The antimicrobial activity of the wires tested was impressive and extensive. The electrochemically etched wires showed a much greater antimicrobial effect when compared

to the standard 99.9% Au and 50/50 % AgAu wires. The images provided in the disk diffusion section portray a consistent and effective antimicrobial effect on both E. coli and S. aureus. The electrochemically etched wires showed a zone of inhibition between 3.7-4.9 mm compared to 0-1.0 mm for the non-etched wires. The likely reason for this effect was the ability of the silver to diffuse easier and more rapidly from the porous structure. Another possibility for the increased activity would be impurities in the wire retained from the etching process. Although the EDS data showed no such impurities, it would still be possible that there exists substances that would have an antimicrobial effect. Further work in the area of characterizing the exact contents of the wire and the leachate seen in the 35x images of the wires on the agar. The leachate and components of the material that is through the entire wire would need to be classified with both chemical analysis as well as with cytotoxicity measurements. The wires would need to be tested to ensure that they do not inhibit growth of all organisms, and not simply the two bacteria strains described in this thesis.

- *Produce thin films of gold and silver alloys with a range of silver content in a reliable and reproducible method*

The thin films produced with metal alloys were created in order to expand the potential uses and applications of the nanoporous metal. In order to create the thin films, PLD was used to create consistent and reliable films containing gold and silver in thicknesses of 135 nm. The process was tested by using profilometry to ensure the linear growth of the thin films and was confirmed by the SEM images of the surface. The textured and dimpled

surface of the thin films was also confirmed with the XRD data that showed crystal growth in the 111 direction indicating epitaxial growth.

The EDS data produced another confirmation of the composition of the thin films created. The 50/50 % AgAu sample was the only sample that was significantly different from the expected composition with a 32/68 % AgAu. This was most likely due to the difficulty of the system to produce a consistent alloy. The EDS method is to select a small region to image and analyze the content of that section. The section used for the EDS measurement could have had a much higher composition of Ag that was not present in the macro sample. Another possible error could have occurred in the production of the target material used for the film growth. The sections that were ablated by the laser during PLD could have had higher concentrations of Ag that were not representative of the entire target material.

Further work should be focused on creating films on uneven and non-silicon wafer substrates. In order to be included in a clinical or surgical application, the films would need to be able to be applied to a wide range of geometries.

- *Measure antimicrobial activity of the thin film alloys*

The thin film alloys that were created through PLD were also tested for their antimicrobial activity using the disk diffusion protocol. Compared to the silicon control, the thin film samples showed an increase in antimicrobial activity as the percentage of silver increased in the sample composition. This relationship was expected and was confirmed by the increased size in the zone of inhibition of the samples. Increasing the sample size and

repetitions of the testing would be the next step for this testing as the n=1 is insufficient to determine the wide ranging effect on antimicrobial effectiveness.

Further work in thin films should also focus on the ability to measure the cytotoxic effect of a pure gold and silver film. The ability to incorporate films such as ones created for this thesis into medical devices is dependent on the ability of the films to not exhibit a negative cell response from healthy human cells.

An area to further investigate would be to combine the effectiveness of the etched alloy wire with the application possibilities of the thin films. A material should be created that is a PLD produced thin film of at least 200 nm thickness and then electrochemically etched to leave approximately 10-20% silver content with 15% the target. A material with the advantages of the thin film along with the advantages of the etched material that would be in between the 10% and 20% silver samples would result in a material with impressive antimicrobial and capacitive behavior. In order to maximize the impact of the electrochemically etched thin film, procedures would need to be developed in order to reduce the variability and difficulty of production that currently exist with the two described methods.

A biomaterial that had the advantages of both electrochemically etched alloy wires and alloy thin films would prove to be medically important. As the applications of gold and silver nanoporous materials increase, research into the effectiveness and ability to reliably control delivery of substances will prove important. Also, with an increasing number of applications of biosensors and microneedle arrays on the surface of skin, it will be important

to minimize the chance of microbial infections or other inflammatory responses to the disturbance of the skin.

VI. REFERENCES

Aden M, Kreutz and Voss A (1993), 'Laser-induced plasma formation during pulsed laser deposition', *Journal of Physics D: Applied Physics*, 26, 1545-1553.

Alfonta L, Bukelman O, Chandra A, Fahrner W, Fink D, Fuks D, Golovanov V, Hnatowicz V, Hoppe K, Kiv A, Klinkovich I, Landau M, Morante J, Tkachenko N, Vacik J, Valden M (2009), 'Strategies toward advanced ion track-based biosensors', *Radiation Effects & Defects in Solids*, 164, 431-437.

Arvizo R, Thompson M, Pabelick C, Rotello V, Mukherjee P and Prakash Y (2011), 'Gold nanoparticles and airway hyperreactivity', *European Respiratory Journal*, 38, 485.

Bauer A, Perry D and Kirby W (1959), 'Single disc antibiotic sensitivity testing of Staphylococci', *American Medical Association Archives Internal Medicine*, 104, 208–216.

Bauer A, Kirby W, Sherris J and Turck M (1966) 'Antibiotic susceptibility testing by a standardized single disk method', *American Journal Clinical Pathology*, 36, 493-496.

Biener J, Hodge A, Hayes J, Volkert C, Zepeda-Ruiz L, Hamza A and Abraham F (2006), 'Size effects on the mechanical behavior of nanoporous Au', *Nano Letters*, 6, 2379-2382.

Cattarin S, Kramer D, Lui A and Musiani M (2007), 'Preparation and characterization of gold nanostructures of controlled dimension by electrochemical techniques', *Journal of Physical Chemistry*, 111, 12643-12649.

Clinical Laboratory Standards Institute (2006), 'Performance standards for antimicrobial disk susceptibility tests', *Approved standard—9th ed. CLSI document M2-A9. 26:1. Clinical Laboratory Standards Institute*, Wayne, PA.

Dersch R, Steinhart M, Boudriot U, Greiner A and Wendorff J (2005), 'Nanoprocessing of polymers: applications in medicine, sensors, catalysis, photonics', *Polymers for Advanced Technologies*, 16, 276-282.

Dong H and Cao X (2009), 'Nanoporous gold thin film: fabrication, structure evolution, and electrocatalytic activity', *Journal of Physical Chemistry*, 113, 603-609.

Forty A (1979), 'Corrosion micromorphology of noble metal alloys and depletion gilding', *Nature*, 282, 597-598.

Ganeev R, Chakravarty U, Naik P, Srivastava H, Mukherjee C, Tiwari M, Nandedkar R and Gupta P (2007), 'Pulsed laser deposition of metal films and nanoparticles in vacuum using subnanosecond laser pulses', *Applied Optics*, 46, 1205-1210.

Gittard S, Pierson B, Ha C, Wu C, Narayan R and Robinson D (2010), 'Supercapacitive transport of pharmacologic agents using nanoporous gold electrodes', *Biotechnology Journal*, 5, 192-200.

Jin H, Kurmanaeva L, Schmauch J, Rosner H, Ivanisenko Y and Weissmuller J (2009), 'Defoming nanoporous metal: role of lattice coherency', *Acta Materialia*, 57, 2665-2672.

Jorgensen J and Turnidge J (2007), 'Susceptibility test methods: dilution and disk diffusion methods', *Manual of Clinical Microbiology*, 9, 1152–1172.

Kafi A, Ahmadalinezhad A, Wang J, Thomas D and Chen A (2010), 'Direct growth of nanoporous Au and its applications in electrochemical biosensing', *Biosensors and Bioelectronics*, 25, 2458-2463.

Kertis F, Snyder J, Govada L, Khurshid S, Chayen N and Erlebacher J (2010), 'Structure/processing relationships in the fabrication of nanoporous gold', *JOM*, 62, 50-56.

Kirby W, Yoshihara G, Sundsted K and Warren J (1957), 'Clinical usefulness of a single disc method for antibiotic sensitivity testing', *Antibiotics Annual*, 892.

Lee J, Park J and Prausnitz M (2008), 'Dissolving microneedles for transdermal drug delivery', *Biomaterials*, 29, 2113-2124.

Liu Z and Searson P (2006), 'Single nanoporous gold nanowire sensors', *The Journal of Physical Chemistry B*, 110, 4318-4322.

Mathur A and Erlebacher J (2007), 'Size dependence of effective Young's modulus of nanoporous gold', *Applied Physics Letters*, 90, 061910-061913.

Pedersen M, Larsen A, Pedersen D, Stoltenberg M and Penkowa M (2009), 'Metallic gold treatment reduces proliferation of inflammatory cells, increases expression of VEGF and FGF, and stimulates cell proliferation in the subventricular zone following experimental traumatic brain injury', *Histology and Histopathology*, 24, 573-586.

Qiu H, Xue L, Ji G, Zhou G, Huang X, Qu Y and Peiji G (2009), 'Enzyme-modified nanoporous gold-based electrochemical biosensors', *Biosensors and Bioelectronics*, 24, 3014-3018.

Quan X, Fischer L, Boisen A, Tenje M (2011), 'Development of nanoporous gold electrodes for electrochemical applications', *Microelectronic Engineering*, 88, 2379-2382.

Reddy P, Varaprasad K, Narayana N, Raju K and Reddy N (2012), 'Fabrication of Au and Ag Bi-Metallic Nanocomposite for Antimicrobial Applications', *Journal of Applied Polymer Science*, online.

Robinson D, Wu C, Ong M, Jacobs B, Pierson B (2010), 'Effect of electrolyte and absorbates on charging rates in mesoporous gold electrodes', *Langmuir*, 26, 6797-6803.

Seker E, Gaskins J, Bart-Smith H, Zhu J, Reed M, Zangari G, Kelly R and Begley M (2007), 'The effects of post-fabrication annealing on the mechanical properties of freestanding nanoporous gold structures', *Acta Materialia*, 55, 4593-4602.

Senior N and Newman R (2006), 'Synthesis of tough nanoporous metals by controlled electrolytic dealloying', *Nanotechnology*, 17, 2311-2316.

Snyder J, Livi K and Erlebacher J (2010), 'Dealloying silver/gold alloys in neutral silver nitrate solution: porosity evolution, surface composition, and surface oxides', *Journal of The Electrochemical Society*, 155, 464-473.

Sperling R, Gil P, Zhang F, Zanella M and Parak W (2008), 'Biological applications of gold nanoparticles', *Chemical Society Reviews*, 37, 1896-1908.

Spohr R (2005), 'Status of ion track technology - Prospects of single tracks', *Radiation Measurements*, 40, 191-202.

Svarosky S, Borovkov A and Sykes K (2008), 'Cationic gold microparticles for biolistic delivery of nucleic acids', *BioTechniques,* 45, 535-540.

Winn W (2006), 'Konemann's color atlas and diagnostic text of microbiology', *Lippencott Williams & Wilkins Publishers*, 6, 945–1021.

Xia Y, Huang W, Zheng J, Niu Z and Li Z (2011), 'Nonenzymatic amperometric response of glucose on a nanoporous gold film electrode fabricated by a rapid and simple electrochemical method', *Biosensors and Bioelectronics,* 26, 3555-3561.

VII. APPENDIX

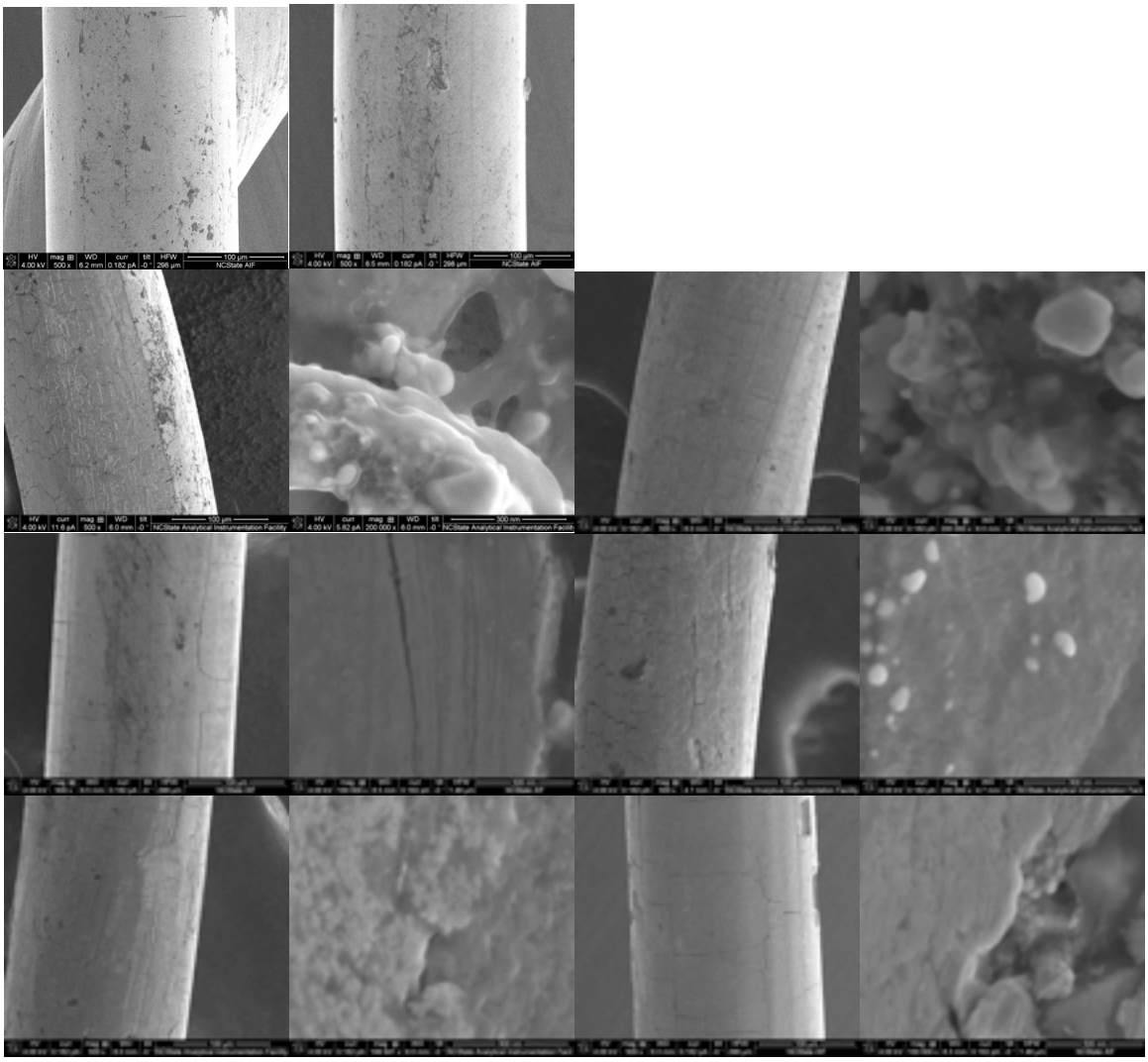

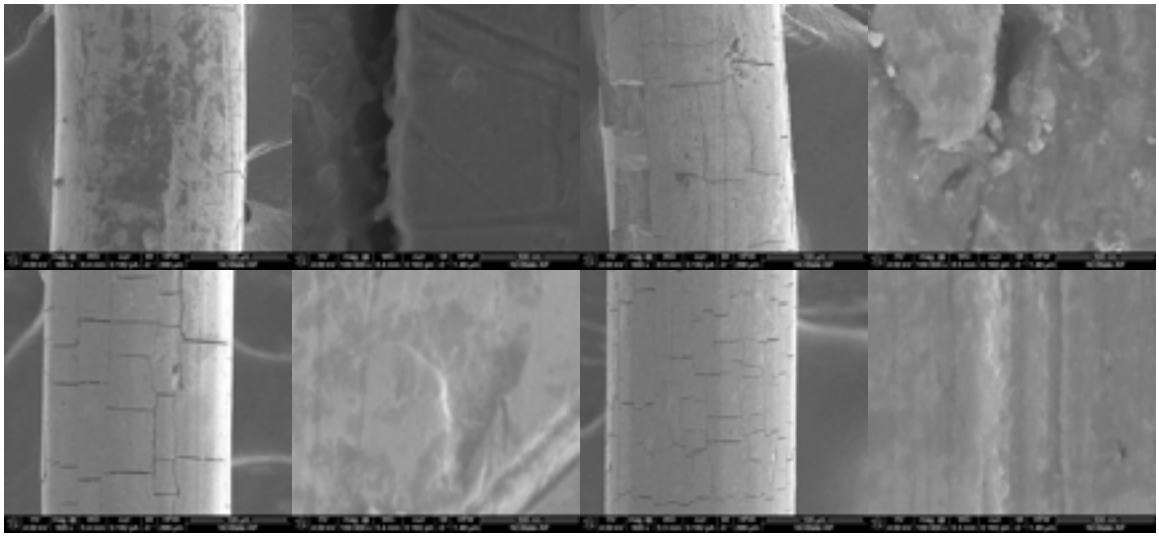

Figure A1. SEM images of all wires.

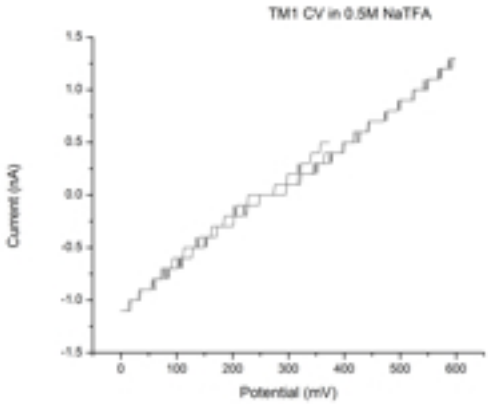
TM1 CV in 0.5M NaTFA
Current (nA)
Potential (mV)

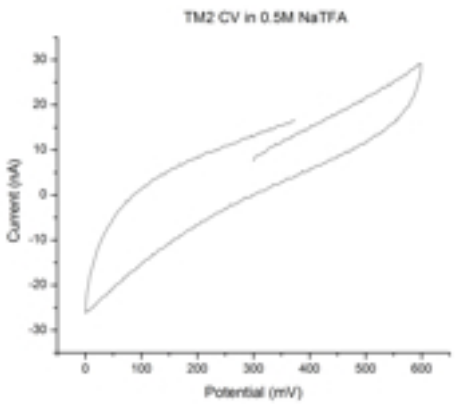
TM2 CV in 0.5M NaTFA
Current (nA)
Potential (mV)

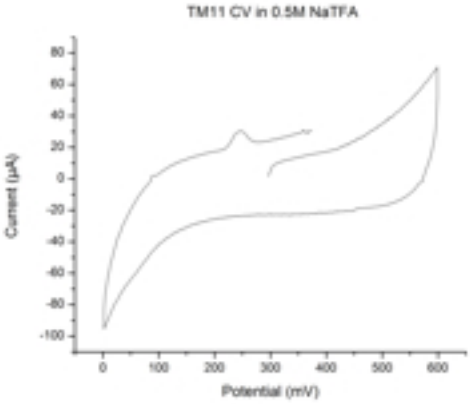
TM11 CV in 0.5M NaTFA
Current (µA)
Potential (mV)

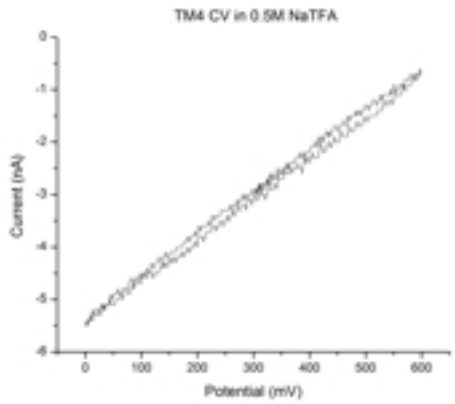
TM4 CV in 0.5M NaTFA
Current (nA)
Potential (mV)

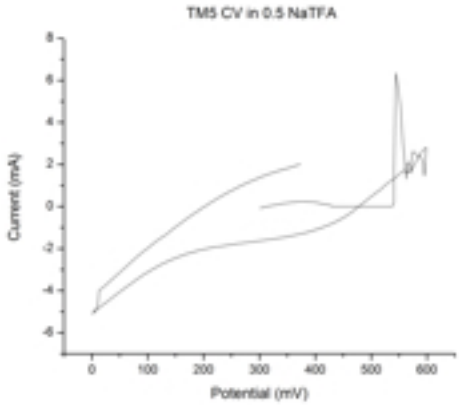
TM5 CV in 0.5 NaTFA
Current (mA)
Potential (mV)

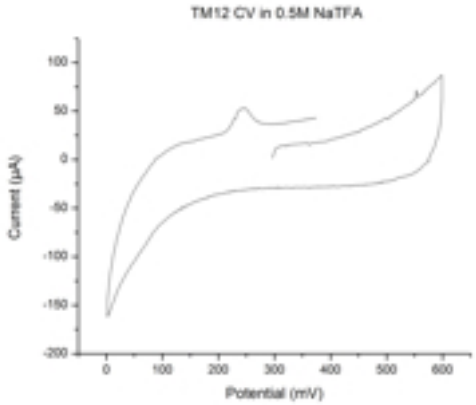
TM12 CV in 0.5M NaTFA
Current (µA)
Potential (mV)

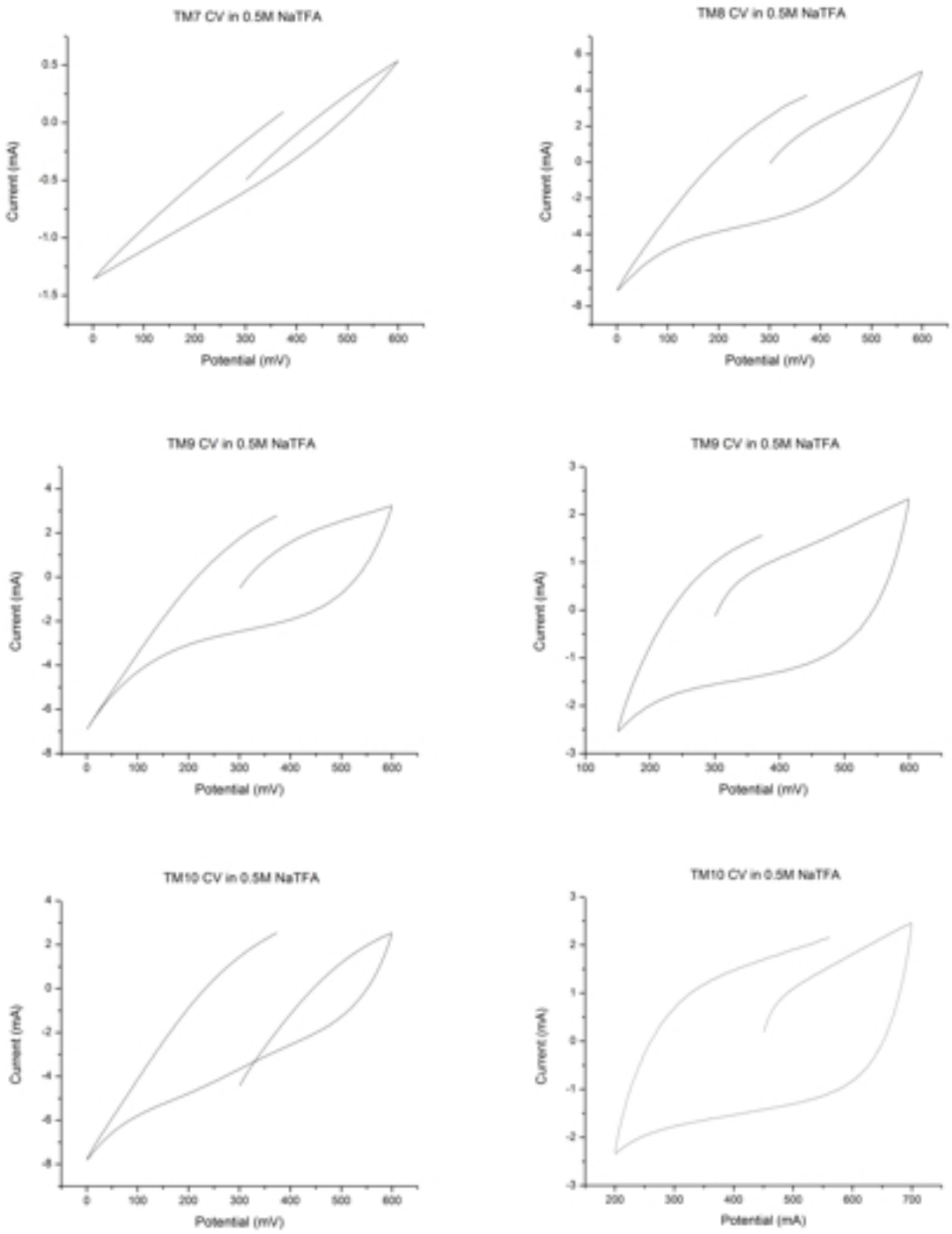

Figure A2. CVs of all wires.

Table A1. All data from disk diffusion.

E. coli	Zone of Inhibition (mm)						
	24 HR						
Wire Photos		1	2	3	4	Avg.	Std. Dev.
50/50 I Wire	Top	0.05	0.00	0.00	0.00	0.01	0.02
	Bottom	0.03	0.04	0.00	0.00	0.02	0.02
						0.01	0.02
100 Au I Wire	Top	0.06	0.09	0.09	0.04	0.07	0.02
	Bottom	0.05	0.04	0.16	0.03	0.07	0.06
						0.07	0.04
TM1	Top	0.46	0.47	0.33	0.43	0.42	0.06
	Bottom	0.40	0.49	0.28	0.51	0.42	0.10
						0.42	0.08
TM4	Top	0.49	0.45	0.44	0.40	0.45	0.04
	Bottom	0.46	0.58	0.48	0.52	0.51	0.05
						0.48	0.04
TM5	Top	0.32	0.44	0.44	0.42	0.40	0.06
	Bottom	0.32	0.49	0.46	0.38	0.41	0.07
						0.41	0.07
TM7	Top	0.34	0.44	0.43	0.45	0.42	0.05

	Bottom	0.39	0.46	0.46	0.42	0.43	0.03
						0.42	0.04
TM9	Top	0.37	0.46	0.54	0.56	0.48	0.09
	Bottom	0.36	0.51	0.58	0.53	0.49	0.10
						0.49	0.09
		Top					
		1	2	3	Avg.	St. Dev.	
Si control	Top	0.00	0.00	0.00	0.00	0.00	
	Right	0.00	0.00	0.00	0.00	0.00	
	Bottom	0.00	0.00	0.00	0.00	0.00	
	Left	0.04	0.00	0.00	0.01	0.02	
					0.00	0.01	
50/50 PLD	Top	0.06	0.06	0.08	0.07	0.01	
	Right	0.06	0.12	0.07	0.08	0.03	
	Bottom	0.13	0.12	0.05	0.10	0.05	
	Left	0.05	0.11	0.07	0.08	0.03	
					0.08	0.03	

75/25 PLD	Top	0.07	0.07	0.11	0.08	0.03	
	Right	0.07	0.22	0.08	0.12	0.08	
	Bottom	0.06	0.18	0.16	0.13	0.06	
	Left	0.06	0.07	0.05	0.06	0.01	
					0.10	0.05	
90/10 PLD	Top	0.15	0.16	0.17	0.16	0.01	
	Right	0.13	0.12	0.13	0.13	0.01	
	Bottom	0.11	0.12	0.11	0.11	0.01	
	Left	0.13	0.11	0.11	0.12	0.01	
					0.13	0.01	
100 Ag PLD	Top	0.12	0.17	0.10	0.13	0.04	
	Right	0.25	0.16	0.17	0.19	0.05	
	Bottom	0.18	0.16	0.14	0.16	0.02	
	Left	0.08	0.11	0.13	0.11	0.02	
					0.15	0.03	
S. aureus	Zone of Inhibition (mm)						

	24 HR						
Wire Photos		1	2	3	4	Avg.	Std. Dev.
50/50 II Wire	Top	0.11	0.12	0.13	0.08	0.11	0.02
	Bottom	0.11	0.10	0.09	0.08	0.10	0.01
						0.10	0.02
100 Au II Wire	Top	0.00	0.04	0.04	0.02	0.02	0.02
	Bottom	0.04	0.03	0.02	0.03	0.03	0.00
						0.03	0.01
TM2	Top	0.35	0.41	0.41	0.47	0.41	0.05
	Bottom	0.35	0.39	0.42	0.46	0.41	0.05
						0.41	0.05
TM8	Top	0.48	0.44	0.39	0.24	0.39	0.10
	Bottom	0.40	0.43	0.33	0.26	0.36	0.08
						0.37	0.09
TM10	Top	0.39	0.43	0.47	0.45	0.43	0.03

	Bottom	0.36	0.42	0.43	0.46	0.42	0.04
						0.43	0.04
TM11	Top	0.44	0.45	0.48	0.38	0.44	0.04
	Bottom	0.44	0.48	0.45	0.38	0.44	0.04
						0.44	0.04
TM12	Top	0.51	0.51	0.49	0.45	0.49	0.03
	Bottom	0.47	0.47	0.47	0.43	0.46	0.02
						0.48	0.02
		1	2	3	Avg.	St. Dev.	
Si control	Top	0.00	0.00	0.00	0.00	0.00	
	Right	0.00	0.00	0.00	0.00	0.00	
	Bottom	0.00	0.00	0.00	0.00	0.00	
	Left	0.00	0.00	0.00	0.00	0.00	
					0.00	0.00	
50/50 PLD	Top	0.02	0.00	0.02	0.01	0.01	
	Right	0.05	0.00	0.02	0.02	0.03	

	Bottom	0.00	0.08	0.00	0.03	0.05	
	Left	0.00	0.02	0.00	0.01	0.01	
					0.02	0.02	
75/25 PLD	Top	0.00	0.00	0.00	0.00	0.00	
	Right	0.00	0.00	0.00	0.00	0.00	
	Bottom	0.00	0.00	0.00	0.00	0.00	
	Left	0.01	0.00	0.00	0.00	0.00	
					0.00	0.00	
90/10 PLD	Top	0.03	0.05	0.02	0.04	0.02	
	Right	0.08	0.07	0.06	0.07	0.01	
	Bottom	0.10	0.08	0.08	0.09	0.02	
	Left	0.00	0.00	0.00	0.00	0.00	
					0.05	0.01	
100 Ag PLD	Top	0.10	0.10	0.07	0.09	0.01	

	Right	0.07	0.07	0.10	0.08	0.02	
	Bottom	0.07	0.05	0.07	0.06	0.02	
	Left	0.08	0.07	0.06	0.07	0.01	
					0.08	0.01	

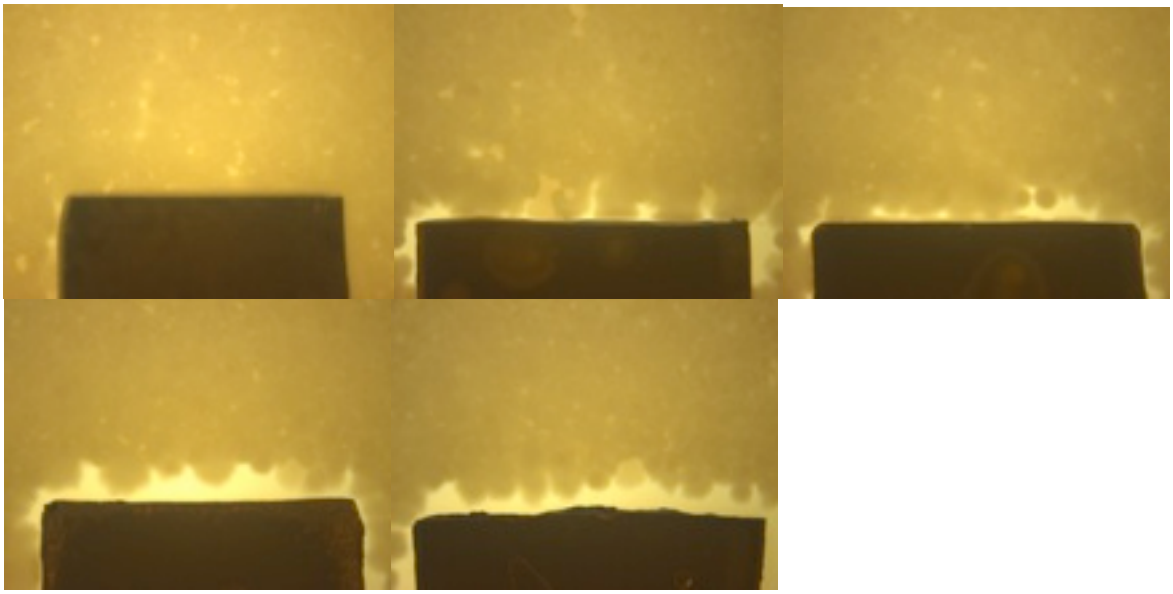

Figure A3. E. coli disk diffusion with PLD samples. Clockwise from top left: Silicon control, 50/50 % AgAu , 75/25 % AgAu, 90/10 % AgAu , 99.9 % Ag.

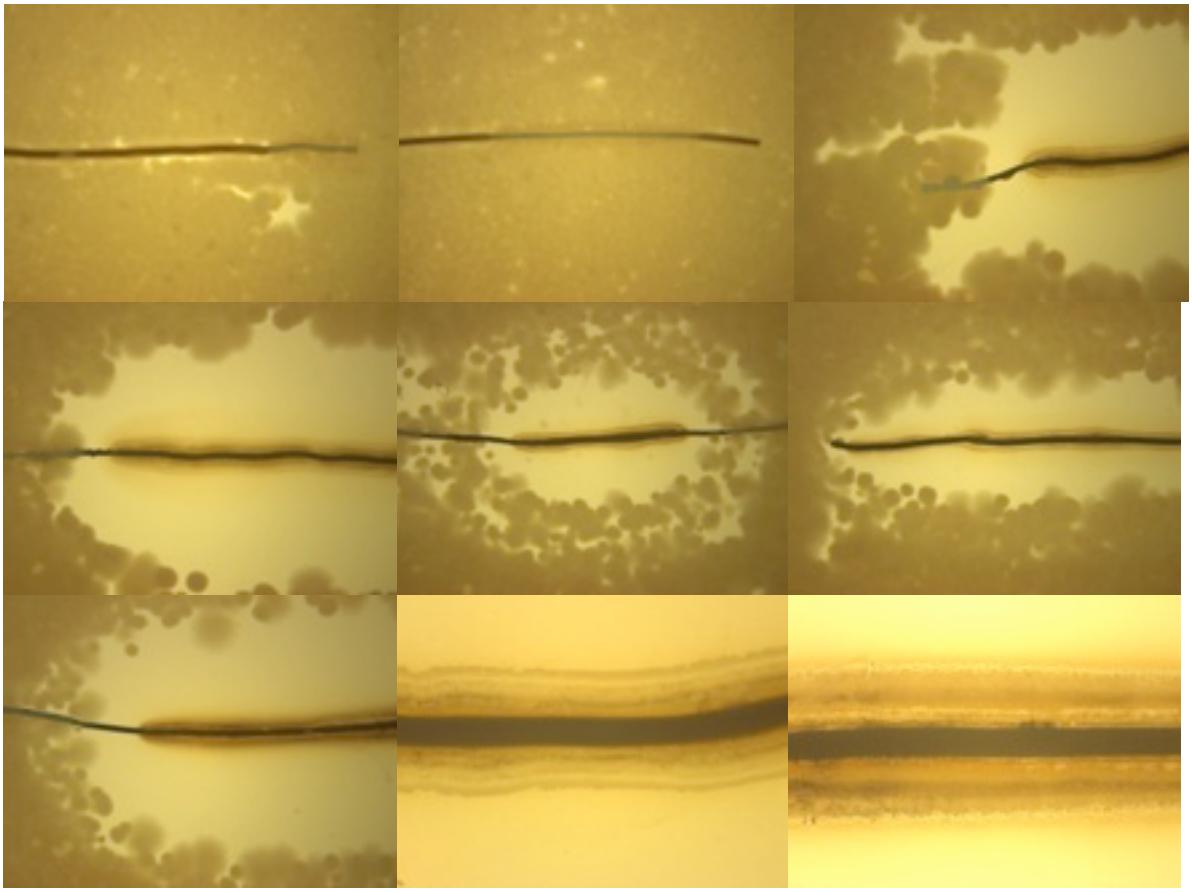

Figure A4. E. coli disk diffusion with etched wires, at 8x. From left to right, starting from top left: 99.9 % Au I Wire, 50/50 % AgAu I Wire (not etched), TM1, TM4, TM5, TM7, TM9, TM1 (35x), TM9 (35x).

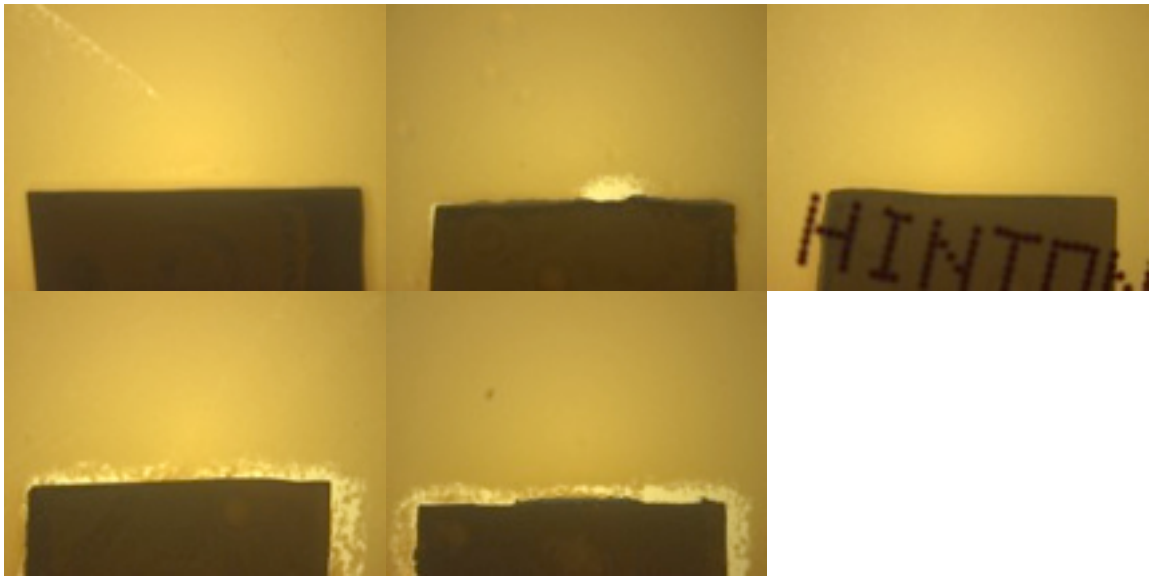

Figure A5. S. aureus disk diffusion with PLD samples. Clockwise from top left: Silicon control, 50/50 % AgAu , 75/25 % AgAu, 90/10 % AgAu , 99.9 % Ag.

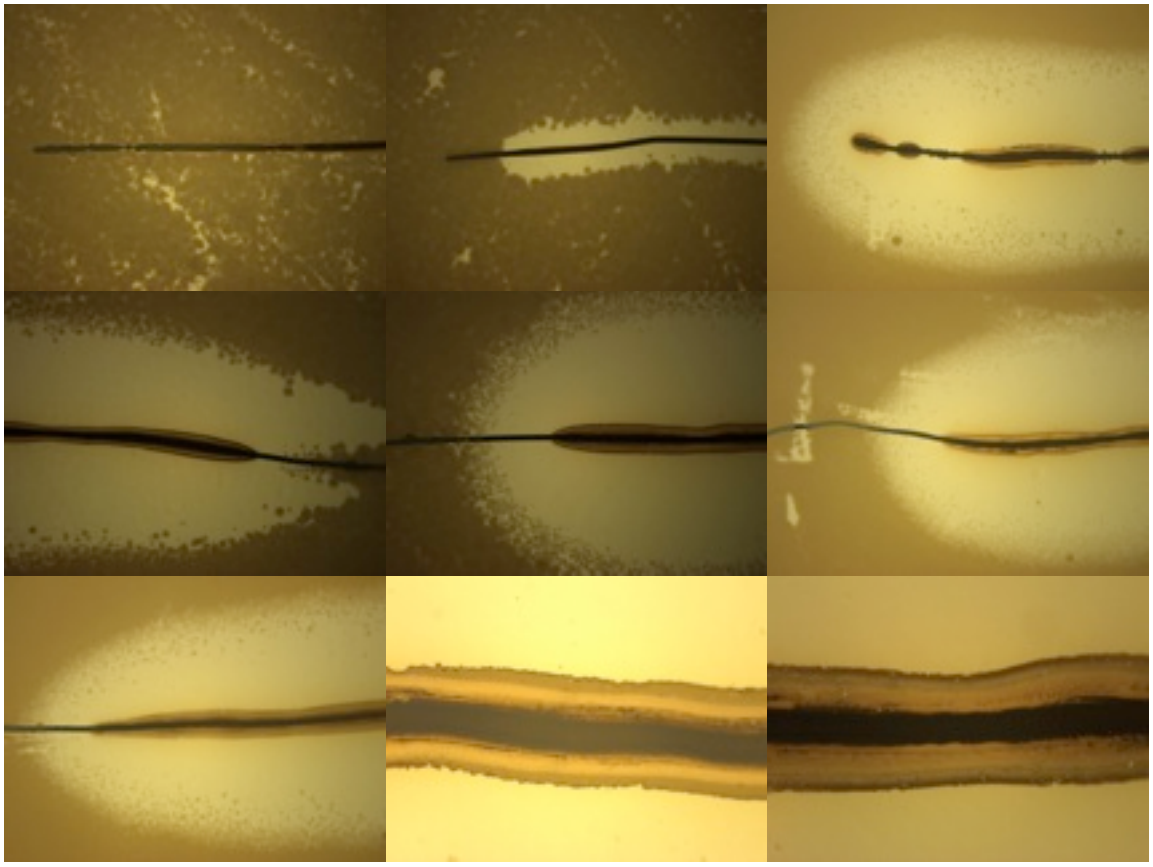

Figure A6. S. aureus disk diffusion with etched wires, at 8x. From left to right, starting from top left: 99.9 % Au II Wire, 50/50 % AgAu II Wire (not etched), TM2, TM11, TM12, TM8, TM10, TM2 (35x), TM12 (35x).